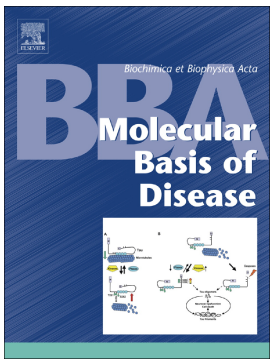

Pre-pregnancy maternal obesity associates with endoplasmic reticulum stress in human umbilical vein endothelium

Roberto Villalobos-Labra, PabloJ. Sáez, Mario Subiabre, Luis Silva, Fernando Toledo, Francisco Westermeier, Fabián Pardo, Marcelo Farías, Luis Sobrevia

PII: S0925-4439(18)30247-3
DOI: doi:10.1016/j.bbadis.2018.07.007
Reference: BBADIS 65177

To appear in: *BBA - Molecular Basis of Disease*

Received date: 9 April 2018
Revised date: 23 June 2018
Accepted date: 6 July 2018

Please cite this article as: Roberto Villalobos-Labra, PabloJ. Sáez, Mario Subiabre, Luis Silva, Fernando Toledo, Francisco Westermeier, Fabián Pardo, Marcelo Farías, Luis Sobrevia , Pre-pregnancy maternal obesity associates with endoplasmic reticulum stress in human umbilical vein endothelium. Bbadis (2018), doi:10.1016/j.bbadis.2018.07.007

Pre-pregnancy maternal obesity associates with endoplasmic reticulum stress in human umbilical vein endothelium

[1]Roberto Villalobos-Labra, [†]Pablo J Sáez, [1]Mario Subiabre, [1,2]Luis Silva, [1,3]Fernando Toledo, [‡]Francisco Westermeier, [1,4]Fabián Pardo, [1]*Marcelo Farías, [1,5,6] *Luis Sobrevia

[1] Cellular and Molecular Physiology Laboratory (CMPL), Division of Obstetrics and Gynaecology, School of Medicine, Faculty of Medicine, Pontificia Universidad Católica de Chile, Santiago 8330024, Chile. [2] Immunoendocrinology, Division of Medical Biology, Department of Pathology and Medical Biology, University of Groningen, University Medical Center Groningen (UMCG), Groningen 9700 RB, The Netherlands. [3] Department of Basic Sciences, Faculty of Sciences, Universidad del Bío-Bío, Chillán 3780000, Chile. [4] Metabolic Diseases Research Laboratory, Center of Research, Development and Innovation in Health - Aconcagua Valley, San Felipe Campus, School of Medicine, Faculty of Medicine, Universidad de Valparaíso, San Felipe 2172972, Chile. [5] Department of Physiology, Faculty of Pharmacy, Universidad de Sevilla, Seville E-41012, Spain. [6] University of Queensland Centre for Clinical Research (UQCCR), Faculty of Medicine and Biomedical Sciences, University of Queensland, Herston, QLD 4029, Queensland, Australia.

Short title: Pre-pregnancy maternal obesity and endothelial ER stress

***Correspondence**: Professor Luis Sobrevia, Dr Marcelo Farías
Cellular and Molecular Physiology Laboratory (CMPL)
Division of Obstetrics and Gynaecology School of Medicine
Faculty of Medicine Pontificia Universidad Católica de Chile
P.O. Box 114-D, Santiago 8330024, Chile.
Telephone: +562-23548117, Fax: +562-26321924
E-mails: lsobrevia@uc.cl, mfarias@med.puc.cl

† **Present address**: Institut Curie, Paris Sciences & Lettres Research University, CNRS, UMR 144, F-75005 Paris, France.

‡ **Present address**: FH JOANNEUM Gesellschaft mbH University of Applied Sciences, Institute of Biomedical Science, Eggenberger Allee 13, 8020 Graz, Austria.

Abstract

Obesity associates with the endoplasmic reticulum (ER) stress-induced endothelial dysfunction. Pregnant women with pre-pregnancy maternal obesity (PGMO) may transfer this potential risk to their offspring; however, whether ER stress occurs and associates with foetoplacental endothelial dysfunction in PGMO is unknown. We studied the L-arginine transport and nitric oxide (NO) synthesis in human umbilical vein endothelial cells (HUVECs) from women with PGMO or with a normal pre-pregnancy weight. We analysed the expression and activation of the ER stress sensors protein kinase RNA-like endoplasmic reticulum kinase (PERK), inositol-requiring enzyme 1α (IRE1α), and activating transcription factor 6 (ATF6). PGMO associated with lower endothelial NO synthase activity due to increased Thr^{495}-inhibitor and decreased Ser^{1177}-stimulator phosphorylation. However, higher expression and activity of the human cationic amino acid transporter 1 was found. PGMO caused activation of PERK and its downstream targets eukaryotic initiation factor 2 (eIF2α), C/EBP homologous protein 10 (CHOP), and tribbles-like protein 3 (TRB3). Increased IRE1α protein abundance (but not its phosphorylation or X-box binding protein 1-mRNA splicing) and increased c-Jun N-terminal kinase 1 phosphorylation was seen in PGMO. A preferential nuclear location of the activating transcription factor 6 (ATF6) was found in HUVECs from PGMO. All the changes seen in PGMO were blocked by TUDCA but unaltered by tunicamycin. Thus, PGMO may determine a state of ER stress via upregulation of the PERK–eIF2α–CHOP–TRB3 axis signalling in HUVECs. This phenomenon results in foetoplacental vascular endothelial dysfunction at birth.

Keywords: obesity; pre-pregnancy; endoplasmic reticulum stress; endothelium; arginine; nitric oxide

Abbreviations

PGMO	Pre-gestational maternal obesity
PGMN	Pre-gestational maternal normal weight
HUVECs	Human umbilical vein endothelial cells
NO	Nitric oxide
NOS	Nitric oxide synthase
eNOS	Endothelial nitric oxide synthase
Akt	Protein kinase B/Akt
ER	Endoplasmic reticulum
UPR	Unfolded protein response
PERK	RNA-like endoplasmic reticulum kinase
IRE1α	Inositol-requiring enzyme 1-alpha
ATF6	Activating transcription factor 6
hCAT-1	Human cationic amino transporter 1
JNK1	c-Jun N-terminal kinase 1
TRB3	Tribbles-like protein 3
CHOP	C/EBP homologous protein 10
BIP	Binding immunoglobulin protein
NBCS	Newborn calf serum
FCS	Foetal calf serum
L-NAME	N^G-Nitro-L-arginine methyl ester
DAF-FM	4-Amino-5-methylamino-2',7'-difluorofluorescein
BMI	Body mass index
TUDCA	Tauroursodeoxycholic acid
OGTT	Oral glucose tolerance test
PBS	Phosphate buffer solution
PCM	Primary culture medium
SDS	Sodium dodecylsulphate
BSA	Bovine serum albumin
HSP90	Heat-shock protein 90

1. Introduction

Obesity is considered an epidemic in developing and developed countries [1]. Pre-gestational maternal obesity (PGMO) characterizes by women with a body mass index (BMI) ≥30 kg/m^2 [1] and is a risk factor for infant and adolescent obesity [2]. PGMO is also associated with the development of metabolic syndrome and increased risk of cardiovascular disease in adulthood [3–5]. Even when the placental transfer of harmful factors from obese mothers to children is known [6–8], the mechanism(s) involved in the maternal-*to*-foetal transfer of risk for PGMO-associated diseases is not fully understood [7,9]. Endothelial dysfunction is a key phenomenon in cardiovascular disease [10]. Maternal obesity has been associated with altered foetoplacental [11] and endothelial dysfunction seen as a reduced response to endothelium-dependent vasodilators [12] and endothelial nitric oxide synthase (eNOS) activation and nitric oxide (NO) generation, likely due to reduced protein kinase B/Akt (Akt) activity [9], in human umbilical vein endothelial cells (HUVECs) [12]. However, nothing is reported regarding PGMO effect on the foetoplacental endothelial function.

Obese subjects show over-activation of the unfolded protein response (UPR) in the antecubital vein endothelial cells suggesting a condition of endoplasmic reticulum (ER) stress [13]. ER stress is induced by stimuli such as accumulation of unfolded proteins, fatty acids, cytokines, redox state dysregulation, or increased intracellular Ca^{2+} levels [14]. ER stress also triggers a UPR following activation of three canonical ER stress sensors, i.e., protein kinase RNA-like endoplasmic reticulum kinase (PERK), inositol-requiring enzyme 1α (IRE1α), and activating transcription factor 6 (ATF6) [14]. These ER stress sensors initiate differential downstream cell signalling sharing common pathways that lead to prosurvival or proapoptotic responses [15]. Antecubital vein endothelial cells from non-

pregnant obese women show higher IRE1 expression, PERK phosphorylation, and ATF6 nuclear localization [13]. ER stress also reduced eNOS activation and NO generation in HUVECs [16] and associated with endothelial dysfunction and reduced insulin response in mouse mesenteric [17] and coronary [18] arteries. Also, skeletal muscle from pregnant women with PGMO presents with ER stress [19]. However, whether PGMO causes ER stress sensors activation in the foetoplacental vascular endothelium is unknown. We hypothesize that ER stress is likely in the foetoplacental endothelium from PGMO pregnancies leading to endothelial dysfunction in this vascular bed. We evaluated the activation of UPR proteins and the effect of ER stress on the L-arginine transport and NO synthesis in HUVECs from PGMO.

2. Material and methods

2.1 Antibodies and materials

Primary monoclonal mouse *anti*-hCAT-1 and *anti*-ß-actin were from Sigma Aldrich (St Louis, MO, USA). Primary polyclonal rabbit *anti*-total eIF2α and *anti*-eIF2α phosphorylated at Ser^{51}, and rabbit *anti*-total Akt and *anti*-Akt phosphorylated at Ser^{473} were from Cell Signaling Technology, Inc. (Danvers, MA, USA). Primary monoclonal mouse *anti*-eNOS phosphorylated at $serine^{1177}$ and *anti*-eNOS phosphorylated at $threonine^{495}$ were from BD Transduction Laboratories (Franklin Lakes, NJ, USA). Primary polyclonal rabbit *anti*-ATF6, *anti*-total IRE1α, *anti*-IRE1α phosphorylated at Ser^{724}, *anti*-total JNK1 and *anti*-JNK1 phosphorylated at Thr^{183}/Tyr^{185} were from Abcam (Cambridge, UK). Polyclonal rabbit *anti*-TRB3 was from Merck Millipore (Billirica, MA, USA). Polyclonal rabbit *anti*-total PERK, *anti*-PERK phosphorylated at Thr^{981}, *anti*-total eNOS, *anti*-CHOP, and secondary horseradish peroxidase-conjugated goat *anti*-rabbit or *anti*-

mouse antibodies were from Santa Cruz Biotechnology (Santa Cruz, CA, USA). For isolation of HUVECs from umbilical cords, Collagenase Type II from *Clostridium histolyticum* (Boehringer, Mannheim, FRG) was used. Medium M199, newborn (NBCS) and fetal calf (FCS) sera, L-glutamine, and penicillin-streptomycin were from Gibco Life Technologies (Carlsbad, CA, USA). L-[^{3}H]Arginine and D-[^{3}H]mannitol were from NEN (Dreieich, FRG). N^G-Nitro-L-arginine methyl ester (L-NAME) was from Sigma Aldrich. Immobilon-P polyvinylidene difluoride membranes were from BioRad Laboratories (Hertfordshire, UK). Qiagen RNAeasy kit was from Qiagen (Crawley, UK) and brilliant SYBR green qPCR Master Mix from Stratagene (La Jolla, CA, USA). The fluorescent dye 4-amino-5-methylamino-2',7'-difluorofluorescein (DAF-FM), tauroursodeoxycholic acid (TUDCA), and tunicamycin were from Merck Millipore (Billirica, MA, USA).

2.2 Study groups

Pregnant women with pre-pregnancy normal weight (n = 20) (hereafter referred as 'PGMN', BMI 18.5–24.9 kg/m^2) or with pre-pregnancy obesity (n = 22) (hereafter referred as 'PGMO', BMI ≥30 kg/m^2) [1,20] were included in this study. PGMN group was selected based on the following exclusion criteria: pre-pregnancy maternal overweight (BMI 25–29.9 kg/m^2) or obesity, previous multiple pregnancies, foetal malformations, hypertensive syndrome, preeclampsia, intrauterine growth restriction, pre-pregnancy or gestational diabetes mellitus. The exclusion criteria for PGMO were PGMN or overweight, and the listed exclusion criteria for PGMO. Deliveries by caesarean section were excluded from the study groups. Therefore, all deliveries were full-term normal vaginal deliveries. Pregnant women included in this study did not smoke or consume drugs or alcohol and had no

intrauterine infection or any other medical or obstetrical complications. The ethnicity of patients included in this study was Hispanic. The investigation conforms to the principles outlined in the Declaration of Helsinki and counts with Ethics Committee approval from the Faculty of Medicine of the Pontificia Universidad Católica de Chile. Patient written, informed consents were obtained 12-24 h before delivery.

The weight of the women before confirming their pregnancy was the one they reported from their own measurements. All pregnant women were evaluated for weight and height, and BMI was recorded at the first interview with the treating obstetrician (i.e., 5–12 weeks of gestation, 1st trimester of pregnancy), then at the 2nd (14–28 weeks of gestation) and 3rd (28–40 weeks of gestation) trimesters of pregnancy, and at delivery (37.1-41 weeks of gestation). Pregnant women with a normal glycaemia at the first trimester of pregnancy were also evaluated by an oral glucose tolerance test (OGTT) with a unique glucose load (75 g fasting) at 24-28 weeks of gestation to discard gestational diabetes mellitus (according to the Perinatal Guide 2015 from the Health Ministry of Chile) [21]. A basal glycaemia <5.55 mmol/L (<100 mg/dL) after 8-9 h from last feeding and <7.9 mmol/L (<140 mg/dL) at 2 h after glucose load was considered as normal [21].

2.3 Human placenta and umbilical cords

Placentas were collected at delivery on ice and transferred to the laboratory until use 15-30 min later. Middle sections of umbilical cords (100-120 mm length) were dissected into 200 mL phosphate-buffered saline (PBS) solution (mmol/L: 130 NaCl, 2.7 KCl, 0.8 Na_2HPO_4, 1.4 KH_2PO_4, pH 7.4, 4ºC) and kept in this solution until use 6-12 h later for isolation of endothelial cells as described [22].

2.4 *Cell culture*

HUVECs were isolated by collagenase digestion (0.25 mg/mL collagenase) from umbilical cords obtained at birth from PGMN or PGMO pregnancies and cultured (37°C, 5% CO_2) in 1% gelatin-coated Petri dishes (100 mm diameter) up to passage 3 in primary culture medium (PCM; M199 containing 5 mmol/L D-glucose, 10% NBCS, 10% FCS, 3.2 mmol/L L-glutamine, and 100 U/mL penicillin-streptomycin) [12,22]. Twelve hours prior experiments the incubation medium was changed to M199 medium containing 1% NBCS and 1% FCS. Cells isolation and culture was done in parallel placentas, i.e., one PGMO with its corresponding PGMN, taken from the total number of samples for each condition (i.e., n = 20 from pregnant women with PGMN and n = 22 from pregnant women with PGMO). Experiments were performed in the absence or presence of tunicamycin (5 µmol/L, 8 h, inducer of ER stress) [23], TUDCA (100 µmol/L, 8 h, reducer of ER stress), tunicamycin + TUDCA (8 h) [24], or L-NAME (100 µmol/L, 20 min, NOS inhibitor) [25].

2.5 *L-Arginine uptake and transport kinetics*

L-Arginine uptake for different concentrations of this amino acid (0-1000 µmol/L, 3 µCi/mL L-[^{3}H]arginine, 1 min incubation, 37°C) (hereafter referred as 'overall uptake') was measured in cells from PGMN (n = 12 different women) and PGMO (n = 12 different women) incubated in Krebs solution (mmol/L: 131 NaCl, 5.6 KCl, 25 $NaHCO_3$, 1 NaH_2PO_4, 20 Hepes, 2.5 $CaCl_2$, 1 $MgCl_2$, pH 7.4, 37ºC), as described [22,26]. Overall uptake of L-arginine was defined as the result of the sum of a saturable component plus a nonsaturable, linear component of uptake in the range of L-arginine concentrations used in this study (hereafter referred as a K_D value defined by m•[*Arg*], where m corresponds to

slopes of linear phases of uptake at a given L-arginine concentration [*Arg*]) [22,26]. Cell monolayers were rinsed with ice-cold Krebs to terminate tracer uptake.

The initial rate of uptake (i.e., linear uptake up to 1 min) was derived from the slope of the linear phases of L-arginine uptakes. Values for uptake were adjusted to the one phase exponential association equation considering the least squares fit:

$$v_i = V_m \cdot (1\text{-}e^{\text{-}(k \cdot t)})$$

where v_i is initial velocity, V_m is the highest velocity reached at a given time (t) and L-arginine concentration, and e and k are constants.

The overall uptake vales at initial rates of the whole range of L-arginine concentrations used in this study (i.e., hereafter referred as overall L-arginine transport) was adjusted to the Michaelis-Menten hyperbola plus a nonsaturable, linear component (K_D) as described [22,26]. The saturable transport of L-arginine was derived by subtracting the m•[*Arg*] components from overall transport, and the transport kinetic parameters maximal velocity (V_{max}) and apparent Michaelis-Menten constant (K_m) of transport were calculated [22,26]. Each transport assay was run in duplicate with transport activity expressed as pmol/µg protein/minute. Radioactivity in 0.5N KCl cell digests was determined by liquid scintillation counting, and uptake was corrected for D-[^{3}H]mannitol disintegrations per minute (d.p.m.) in the extracellular space [22].

2.6 Western blotting

Total protein was obtained from confluent cells from PGMN (n = 9 different women) and PGMO (n = 9 different women), washed twice with ice-cold PBS and

harvested in 100 μL of lysis buffer composed by 63.7 mmol/L Tris/HCl (pH 6.8), 10% glycerol, 2% sodium dodecyl sulphate (SDS), 1 mmol/L sodium orthovanadate, 50 mg/mL leupeptin, and 5% 2-mercaptoethanol, as described [22]. Cells were sonicated (6 cycles, 5 s, 100 Watts, 4ºC), and total protein was separated by centrifugation (14000 *g*, 15 min, 4°C). Proteins (70 μg) were separated by SDS-polyacrylamide gel (10%) electrophoresis and transferred onto Immobilon-P polyvinylidene difluoride membranes. The proteins were then probed against hCAT-1 (1:1000 dilution, 12 h, 4ºC), total eNOS (1:1000 dilution, 3 h, room temperature), eNOS phosphorylated at serine^{1177} (P~Ser^{1177}-eNOS, 1:1000 dilution, 12 h, 4ºC), eNOS phosphorylated at threonine^{495} (P~Thr^{495}-eNOS, 1:1000 dilution, 12 h, 4ºC), total Akt (1:1000 dilution, 3 h, room temperature), Akt phosphorylated at serine^{473} (P~Ser^{473}Akt, 1:1000 dilution, 3 h, room temperature), total PERK (1:500 dilution, 12 h, 4°C), PERK phosphorylated at threonine^{981} (P~Thr^{981}PERK, 1:500 dilution, 12 h, 4°C), total eIF2α (1:1000 dilution, 12 h, 4°C), eIF2α phosphorylated at serine^{51} (P~Ser^{51}eIF2α, 1:1000 dilution, 12 h, 4°C), CHOP (1:1000 dilution, 12 h, 4°C), TRB3 (1:1000 dilution, 12 h, 4°C), total IRE1α (1:1000 dilution, 12 h, 4°C), IRE1α phosphorylated at serine^{724} (P~Ser^{724}IRE1α, 1:1000 dilution, 12 h, 4°C), total JNK1 (1:1000 dilution, 12 h, 4°C), JNK1 phosphorylated at threonine^{183} and tyrosine^{185} (P~Thr^{183}/Tyr^{185}JNK1, 1:1000 dilution, 12 h, 4°C), and ß-actin (1:5000, 1 h, room temperature, loading control). Membranes were rinsed in Tris buffer saline plus 0.5% Tween (TBS-T) and incubated (1 h) in TBS-T/0.5% fat-free milk containing secondary horseradish peroxidase-conjugated antibodies. Proteins were detected by enhanced chemiluminescence in a ChemiDoc-It 510 Imagen System (UVP, LCC Upland, CA, USA) at the linear phase of luminescence for each antibody for the target proteins analysed and quantified by densitometry [22].

2.7 Isolation of total RNA and reverse transcription

Total RNA was isolated from PGMN (n = 8 different women) and PGMO (n = 8 different women) using the Qiagen RNAeasy kit. RNA quality and integrity were insured by gel visualization and spectrophotometric analysis ($OD_{260}/_{280}$), quantified at 260 nm as described [22]. Aliquots (2 µg) of total RNA were reversed transcribed into cDNA.

2.8 Quantitative PCR

Experiments were performed using a StepOne Real-Time PCR system (Applied Biosystems, Foster City, CA, USA) in a reaction mix containing 0.5 µmol/L primers, and master mix provided in the brilliant SYBR green qPCR Master Mix as described [22]. Hot-start DNA polymerase was activated (20 s, 95°C), and the PCR cycling profile included a 95ºC denaturation (3 s), annealing (30 s) at 56°C (CHOP, TRB3, BIP, XBP1, and β-actin) and 54ºC (28S), and extension (30 s) at 72ºC. Product melting temperature values were 79.3°C (CHOP), 83.7°C (TRB3), 73.8°C (BIP), 80.2°C (β-actin), and 80ºC (28S). Primers efficiency were 101.5% (CHOP), 91.3% (TRB3), 103.1% (BIP), 93.3% (β-actin), and 109.3% (28S). The oligonucleotide primers used in this study were: CHOP sense: 5'-AATGAACGGCTCAAGCAGGA-3', CHOP *anti*-sense: 5'-TGCAGATTCACCATTCGGTCA-3', TRB3 sense: 5'-ATTAGGCAGGGTCTGTCCTGTG-3', TRB3 *anti*-sense: 5'-AGTATGGACCTGGGATTGTGGA-3', BIP sense 5'-CCACCAAGATGCTGACATTG-3', BIP *anti*-sense: 5'-AGGGCCTGCACTTCCATAGA-3', XBP1 sense: 5'-GGAGTTAAGACAGCGCTTGGGGA-3' XBP1 *anti*-sense: 5'-TGTTCTGGAGGGGTGACAACTGGG-3', β-actin sense: 5'-

GCCGGGACCTGACTGACTAC-3', β-actin *anti*-sense: 5'-TTCTCCTTAATGTCACGCACGAT-3', 28S sense: 5′-TTGAAAATCCGGGGGAGAG-3′, 28S *anti*-sense: 5′-ACATTGTTCCAACATGCCAG-3′. Expected size products were CHOP 89 bp, TRB3 90 bp, BIP 100 bp, β-actin 100 bp, 28S 100 bp, XBP1 164 bp (spliced) and 138 bp (unspliced). The threshold cycle (Ct) value was defined as the PCR cycle number at which the fluorescent signal of the probes exceeded background and was used for calculating gene expression data with the $2^{-\Delta\Delta Ct}$ method [27]. The amplification of the control genes 28S and β-actin was linear between 14–37.5 and 7–35 Ct, respectively. Equally, target genes TRB3, CHOP, and BIP amplification was linear within 5–33, 5–35, and 10–35 Ct, respectively. Experimental samples amplification was linear with 20–26, 26–34, and 18–28 Ct for TRB3, CHOP, and BIP, respectively. Amplification of control genes 28S and β-actin was similar in the experimental groups PGMN and PGMO in the absence or presence of tunicamycin, TUDCA, or both molecules (not shown). For XBP1, the amplified cDNA was separated on a 1.5% agarose gel to differentiate the spliced and unspliced XBP1 cDNA as described [28].

2.9 Intracellular NO determination

Intracellular NO was determined using the fluorescent dye DAF-FM as described [22]. Confluent cells from PGMN (n = 8 different women) and PGMO (n = 8 different women) grown on 100 mm^2 culture plate were incubated in the absence or presence of tunicamycin (5 µmol/L, 8 h) and TUDCA (100 µmol/L, 8 h), and then exposed (1 h, 37ºC) to 5 µmol/L DAF-FM in the absence or presence of 100 µmol/L L-NAME in Krebs buffer (37ºC, pH 7.4). The fraction of NOS-activity derived NO was estimated by the difference

between the fluorescence in the presence and absence of L-NAME. The fluorescence ($\lambda_{exc}/\lambda_{em}$: 485/538 nm) was determined in an Infinite M200PRO Tecan (Männedorf, Zürich, Switzerland).

2.10. NOS activity

The activity of NOS was assayed by quantification of the intracellular content of L-citrulline by high performance liquid chromatography (h.p.l.c.) in HUVECs from PGMN (*n* = 3 different women) and PGMO (*n* = 3 different women) in the absence or presence of 100 μmol/L L-NAME, as described [22].

2.11 Arginase activity

Total urea production from L-arginine was measured as previously described in HUVECs [29]. In brief, total cell protein aliquotes (70 μg contained in 90 μL) obtained from cells from PGMN (*n* = 3 different women) and PGMO (*n* = 3 different women) incubated in the absence or presence of 20 μmol/L *S*-(2-boronoethyl)-L-cysteine (BEC, arginases inhibitor) [30], were preincubated (10 min, 55°C) with 100 mmol/L $MnCl_2$ in 50 mmol/L Tris-HCl (pH 7.5) and then mixed with L-arginine (50 mmol/L, 60 min, 37°C). The reaction was stopped by addition (400 μL) of an acid mix (H_2SO_4:H_3PO_4:H_2O = 1:3:7 v/v) and incubated (45 min, 100°C) with 9% α-isonitrosopropiophenone (25 μL) for colorimetric determination of urea (absorbance at 540 nm) in a microplate reader (Thermo Labsystems, Waltham, MA, USA). Arginases activity was calculated from the urea formation in the absence of BEC minus the urea formation in the presence of this inhibitor [29,30]. Activity was expressed as pmol urea/μg protein/minute.

2.12 Confocal laser scanning microscopy

HUVECs were grown on glass coverslips (6 x10^4 cells per slide) (Sail Brand, Shanghai, China) in PCM to 100% confluence as described [12]. Cells were then cultured in medium M199 containing 1% FCS and 1% NBCS in the absence or presence of tunicamycin (5 µmol/L, 8 h), TUDCA (100 µmol/L, 8 h), or both molecules, then fixed in 4% paraformaldehyde (5 min), rinsed (x3) with PBS, permeabilised, and blocked with 1% BSA-containing blocking solution (50 mmol/L NH_4Cl, and 0.05% Triton X-100 in PBS (2 h) [31]. ATF6 was immunolocalised by incubating the cells with primary monoclonal rabbit *anti*-ATF6 (1:30 dilution) (Spring Bioscience, Pleasanton, CA, USA) overnight at 4°C in 1% BSA-blocking solution. The cells were then washed (x3) with PBS, followed by incubation (1 h, 22°C) with the secondary antibody Alexa Fluor 568 goat *anti*-rabbit IgG (H+L, $\lambda_{exc}/\lambda_{em}$: 578/603 nm, 1:500 dilution) (Life Technologies) in 1% BSA-blocking solution. Nuclei were counterstained with DAPI (5 µmol/L, Life Technologies) and mounted with Fluoromount G (Electron Microscopy Sciences, Washington, PA, USA). Images were acquired under an inverted Eclipse C2 confocal Nikon microscope using a 60x oil immersion objective lens (numerical aperture 1.4) and the confocal acquisition software NIS-Elements C (Nikon, Tokio, Japan). Each sample was examined through successive 0.3 µm optical slices along the z axis to capture 15 slices per cell. Relative fluorescence was measured using ImageJ version 1.52b (Wayne Rasband NIH, USA) [32] and the ratio between the ATF6 fluorescence at the nuclear region and the perinuclear region of each cell was determined. Nuclear regions defined by DAPI fluorescence were also analysed for the optical slide number 7, i.e., ~2.1 µm from cell culture surface. ATF6 fluorescence at the

perinuclear region (*pnA*) was derived from the expression $pnA = (1.9 \cdot nA) - nA$, where *nA* is the nuclear region corresponding to DAPI fluorescence and 1.9 is the increase in the *nA* fixed for each cell analysed.

2.14 Statistical analysis

The sample size was estimated considering a power of 80% enough to detect differences between both groups (based on a two-sided alpha level of 0.05). Values for clinical parameters are given as mean ± S.D. (range). For *in vitro* assays the values are mean ± S.E.M., where *n* indicates the number of different biological samples for which each assay was replicated 2-3 times. Comparisons between two groups were performed by means of Student's unpaired *t*-test or Mann-Whitney test for parametric or non-parametric data, respectively. The differences between more than two groups were performed by analysis of variance (one-way or two-way ANOVA). If ANOVA demonstrated a significant interaction between variables, *post hoc* analyses were performed by the Bonferroni multiple-comparison. The statistical software GraphPad Instat 3.0b and Graphpad Prism 8.0a.91 (GraphPad Software Inc., San Diego, CA, USA) were used for data analysis. $P<0.05$ was considered statistically significant.

3. Results

3.1 Study groups

Pregnancies were a singleton, and pregnant women showed with similar age and height, were normotensive, with similar OGTT and normal glycaemia at delivery (Table 1). The pre-pregnancy weight and BMI were higher in PGMO compared with PGMN. The

total gestational weight gain (*t*GWG) and rate of GWG (*r*GWG) for 2nd to 3rd trimester of pregnancy ($^{2nd\text{-}3rd}$*r*GWG) were within the recommended values for pregnant women with a normal pre-pregnancy BMI (*t*GWG 11.5–16 kg, $^{2nd\text{-}3rd}$*r*GWG ≤0.42 kg per week) or pre-pregnancy obesity (BMI ≥30 kg/m^2) (*t*GWG 5–9 kg, $^{2nd\text{-}3rd}$*r*GWG ≤0.22 kg per week) according to the 2009 US Institute of Medicine (IOM) guidelines (IOM, 2009).

The *t*GWG was higher (2.18 ± 0.9 fold) in PGMN compared with PGMO (Table 1). Women from the PGMN group show an increase but from the PGMO group show a decrease in the GWG change (ΔGWG) between pre-pregnancy and the 1st trimester of pregnancy ($^{Pp–1st}$ΔGWG). However, the ΔGWG was lower for 1st to 2nd ($^{1st\text{-}2nd}$ΔGWG) and 3rd trimester of pregnancy to delivery ($^{3rd–Del}$GWG), but it was similar for 2nd to 3rd trimester of pregnancy ($^{2nd\text{-}3rd}$ΔGWG) in both groups of women. Similar findings were seen for the *r*GWG in women from these two groups. The total change in the BMI (ΔBMI) between pre-pregnancy and delivery was higher in PGMN compared with PGMO (Table 1). In women from the PGMO group, a maximal increase was seen at $^{1st\text{-}2nd}$ΔBMI with a lower increase in this parameter up to delivery. However, women from the PGMO group showed a decrease in the $^{Pp–1st}$BMI with a negative $^{Pp\text{-}1st}$ΔBMI value followed by a continuous increase up to delivery. The ΔBMI was lower for $^{1st\text{-}2nd}$ΔBMI and $^{3rd\text{-}Del}$ΔBMI, but it was similar in $^{2nd\text{-}3rd}$ΔBMI in both groups of women. Clinical parameters of newborns from the two study groups did not show significant differences.

3.2 L-Arginine transport kinetics and hCAT-1 expression

The v_i for overall 100 µmol/L L-arginine transport was linear up to 60 seconds in cells from PGMN and PGMO pregnancies in the absence or presence of tunicamycin,

TUDCA, or both molecules (not shown). Values for v_i were higher in cells from PGMO compared with PGMN (Table 2). Tunicamycin increased the v_i in cells from PGMN to values close to those in cells from PGMO; however, did not alter this parameter in cells from PGMO. TUDCA reversed the increase seen in the v_i in cells from PGMO in the absence or presence of tunicamycin and in cells from PGMN incubated with tunicamycin. However, TUDCA did not alter the v_i in cells from PGMN in the absence of this ER stress inducer.

Overall L-arginine transport in the absence or presence of tunicamycin or TUDCA was semi-saturable and best-fitted by a non-linear representation in Eadie-Hofstee plots in cells from PGMN (Fig. 1A) and PGMO (Fig. 1B). The K_D value was lower in PGMO compared with PGMN in the absence of tunicamycin or TUDCA (Table 2). None of these molecules altered the K_D in cells from PGMN; however, tunicamycin increased the K_D in cells from PGMO pregnancies. TUDCA blocked tunicamycin effect but did not alter the K_D value in the absence of this ER stress inducer in cells from PGMO.

After subtracting the linear, non-saturable transport component from overall transport, the remaining L-arginine transport was saturable, adjusted to a single Michaelis-Menten equation, and linear in an Eadie-Hofstee plot (Fig. 1C,D). The saturable transport in cells from PGMO showed higher V_{max} and maximal transport capacity (V_{max}/K_m) compared with cells from PGMN pregnancies (Table 2). In cells from PGMN, the V_{max} and V_{max}/K_m were increased by tunicamycin, an effect blocked by TUDCA. However, TUDCA did not alter these parameters in these cells. The increased V_{max} and V_{max}/K_m seen in cells from PGMO was unaltered by tunicamycin but blocked by TUDCA in the absence or presence of tunicamycin. The apparent K_m values were not significantly altered in cells from these two study groups in all experimental conditions (Table 2).

The hCAT-1 protein abundance was higher in HUVECs from PGMO compared with PGMN group (Fig. 1E). Incubation of cells from PGMN with tunicamycin increased hCAT-1 protein abundance but unaltered the PGMO-increased abundance of this protein. TUDCA reversed the PGMO-increased hCAT-1 protein abundance in the absence of presence of tunicamycin but did not alter this protein expression in cells from the PGMN group. TUDCA also reversed the increase in the hCAT-1 protein abundance caused by tunicamycin in cells from PGMN.

3.3 NOS and arginase activity, and eNOS and Akt protein abundance

The level of NOS-derived NO detected by fluorescence in DAF-loaded cells was lower in cells from PGMO compared with PGMN pregnancies (Fig. 2A). Tunicamycin decreased the level of NO in cells from PGMN, an effect blocked by TUDCA. The PGMO-decreased NO generation was unaltered by tunicamycin but it was partially reversed by TUDCA. However, the PGMO-reduced NO level was unaltered by TUDCA in cells incubated with tunicamycin. Similar results were found in assays for NOS-activity dependent L-citrulline synthesis by h.p.l.c. (Fig. 2B). However, cells from PGMO showed a more pronounced reduction in the L-citrulline synthesis in the absence (76 ± 7%) or presence (94 ± 5%) of tunicamycin than the NO level detected by the fluorescent assay (38 ± 4 and 37 ± 2%, respectively) compared with cells from PGMN.

Cells from both groups of women show comparable total eNOS protein abundance in the absence or presence of tunicamycin or TUDCA (Fig. 2C). The P~Thr^{495}eNOS protein abundance was higher in cells from PGMO compared with PGMN. Tunicamycin and TUDCA did not alter the P~Thr^{495}eNOS protein abundance in cells from PGMN. The

effect of PGMO on the P~Thr^{495}eNOS protein abundance was unaltered by tunicamycin but reversed by TUDCA, an effect not seen in cells coincubated with this molecule and tunicamycin. In the absence of tunicamycin and TUDCA, the P~Ser^{1177}eNOS protein abundance was lower in cells from PGMO compared with PGMN. Tunicamycin reduced the P~Ser^{1177}eNOS protein abundance in cells from PGMN, an effect that was blocked by TUDCA. The PGMO-reduced P~Ser^{1177}eNOS protein abundance was unaltered by tunicamycin but reversed by TUDCA. The effect of this ER stress reducer was absent in cells from PGMO coincubated with TUDCA + tunicamycin.

Total Akt protein abundance was unaltered by PGMO, tunicamycin or TUDCA (Fig. 2D). However, the P~Ser^{473}Akt protein abundance was lower in cells from PGMO and reduced by tunicamycin in cells from PGMN. TUDCA blocked the effects of PGMO or tunicamycin. Arginase activity, corresponding to the fraction of urea formation inhibited by BEC, was higher in cells from PGMO compared with PGMN pregnancies (Fig. 2E). Tunicamycin increased arginase activity in cells from PGMN, an effect blocked by TUDCA. The PGMO-increased arginase activity was unaltered by tunicamycin but blocked by TUDCA.

3.4. PERK, eIF2α, CHOP, TRB3, and BIP expression

Total PERK protein abundance was similar in cells from both groups of women in the absence or presence of tunicamycin or TUDCA (Fig. 3A). The P~Thr^{981}PERK protein abundance was higher in cells from PGMO compared with PGMN. Tunicamycin increased the P~Thr^{981}PERK protein abundance in cells from PGMN, an effect prevented by TUDCA. However, TUDCA did not alter P~Thr^{981}PERK in these cells. PGMO-increased

P~Thr^{981}PERK protein abundance was unaltered by tunicamycin but blocked by TUDCA in the absence or presence of tunicamycin. A similar pattern of responses for total eIF2α and P~Ser^{51}eIF2α protein abundance was seen in cells from PGMN or PGMO pregnancies (Fig. 3B).

CHOP and TRB3 protein abundance were higher in cells from PGMO compared with PGMN, which was unaltered by tunicamycin but blocked by TUDCA only in the absence of the ER stress inducer (Fig. 3C). Tunicamycin increased the CHOP and TRB3 protein abundance in cells from PGMN, a response blocked by TUDCA in the absence or presence of tunicamycin. The relative mRNA level for CHOP, TRB3, and BIP were higher in cells from PGMO compared with PGMN (Fig. 3D). PGMO-increased CHOP, TRB3, and BIP mRNA levels were unaltered by tunicamycin. TUDCA blocked PGMO effect and the increase caused by tunicamycin in the mRNA level for these genes in cells from PGMN in the absence of this ER stress inducer. Similar results were obtained when target mRNA genes expression was compared against the control gene 28S rRNA (not shown).

3.5 IRE1α and JNK1 expression, and XBP1 mRNA processing

Total IRE1α protein abundance was higher in cells from PGMO compared with PGMN (Fig. 4A). Incubation of cells from PGMN with tunicamycin increased total IRE1α protein abundance but unaltered the PGMO-increased abundance of this protein. TUDCA reversed the PGMO-increased total IRE1α protein abundance in the absence or presence of tunicamycin but did not alter the expression of this protein in cells from the PGMN group. TUDCA also reversed the increase in the total IRE1α protein abundance caused by tunicamycin in cells from PGMN. The P~Ser^{724}IRE1α protein abundance was unaltered by

PGMO or any experimental condition used in this study. The unspliced XBP1 mRNA (164 bp) level was similar in cells from both groups of women (Fig. 4B). Tunicamycin increased the processing of XBP1 mRNA generating a spliced XBP1 mRNA (138 bp), an effect that was similar in PGMO and PGMN.

Total JNK1 protein abundance was unaltered by PGMO, tunicamycin, or TUDCA (Fig. 4C). However, P~Thr^{183}/Tyr^{185}JNK1 protein abundance was higher in cells from PGMO, an effect unaltered by tunicamycin but blocked by TUDCA in the absence or presence of tunicamycin. In cells from PGMN pregnancies, tunicamycin increased the P~Thr^{183}/Tyr^{185}JNK1 protein abundance which was blocked by TUDCA.

3.6 ATF6 activation

Confocal immunofluorescence analysis shows that ATF6 protein is expressed in cells from PGMN (Fig. 5A) and PGMO groups (Fig. 5B). In the absence of tunicamycin or TUDCA, ATF6 was detected mainly at the perinuclear region in cells from PGMN pregnancies (Fig. 5C). However, ATF6 was detected in the nuclear region in cells from PGMO pregnancies. Tunicamycin increased the ATF6 signal at the nuclear region in cells from PGMN but did not alter the nuclear signal for this protein in cells from PGMO. TUDCA did not alter the perinuclear distribution of ATF6 signal in cells from PGMN but abolished the ATF6 signal at the nuclear region in cells from PGMO pregnancies. TUDCA also reduced the tunicamycin-increased signal at the nuclear region resulting in higher perinuclear signal for this protein in cells from PGMN pregnancies. In cells from PGMO pregnancies treated with tunicamycin, TUDCA reduced the nuclear signal for ATF6 protein.

4. Discussion

This study reports that HUVECs from pregnancies with PGMO show increased expression and activation of the major ER stress sensors PERK, IRE1α, ATF6, and BIP. ER stress is a phenomenon that resulted in lower NO synthesis. Thus, PGMO is a deleterious condition altering the foetoplacental vasculature at birth due to the generation of ER stress.

Women with PGMO showed lower total variation of GWG (ΔGWG), and reduced ΔGWG and rate of GWG (*r*GWG) during pregnancy except for 2^{nd}–3^{rd} trimesters compared with women with PGMN. Total GWG (*t*GWG) and *r*GWG for 2^{nd}–3^{rd} trimesters of pregnancy ($rGWG^{2nd\text{-}3rd}$) in women with PGMO was within the recommended values for pregnant women with pre-pregnancy BMI ≥30 kg/m^2 (*t*GWG 5–9 kg, $rGWG^{2nd\text{-}3rd}$ 0.22 kg per week) from the US Institute of Medicine [20]. These findings fit with previous studies showing that women that were obese or overweight before pregnancy showed a *t*GWG and *r*GWG according with the expected values for this group of patients [12,20].

Interestingly, *t*GWG, ΔGWG, and *r*GWG (except for $rGWG^{2nd\text{-}3rd}$) changes in women with PGMO were different from PGMN and compared with women that started pregnancy with normal weight and BMI but showed supraphysiological *r*GWG [12]. Thus, PGMO may refer to a different metabolic condition compared with women with PGMN and supraphysiological *r*GWG. Indeed, PGMO associates with lower bioenergetics performance of human amnion and umbilical cord stem cells [33], higher placental DNA methylation [34], or higher placental lesions of maternal vascular supply [35]. These

PGMO-associated alterations in the placenta result in adverse intrauterine milieu increasing the risk of foetal and newborn disturbances.

4.1 Endothelial L-arginine transport/NO synthesis

The reduced NO synthesis in HUVECs from PGMO is similar to cells from women starting pregnancy with normal weight and BMI but showing supraphysiological *r*GWG [20]. This phenomenon resulted from lower eNOS activity due to higher inhibitor Thr^{495} phosphorylation of this enzyme [12]. PGMO-reduced NO synthesis also associated with reduced eNOS activity, likely due to its lower activator Ser^{1177} in addition to higher inhibitor Thr^{495} phosphorylation. However, PGMO-reduced NO synthesis was not due to lower eNOS protein abundance. Interestingly, reduced NO synthesis in HUVEC from PGMO may result from a lower activation of Akt since its activator phosphorylation at Ser^{473} is reduced compared with cells from PGMN. This finding confirms the involvement of Akt as a key modulator of NOS (including eNOS) activity in HUVECs [9]. A reduced NO bioavailability is also reported in HUVECs from gestational diabetes mellitus pregnancies, a phenomenon that could result from increased level of superoxide anion which acts as scavenger for NO [9,36-38]. This phenomenon is an alternative mechanism by which PGMO may result in reduced NO levels in HUVECs. Thus, PGMO-reduced foetoplacental eNOS activity is via a different mechanism than in women with normal pre-pregnancy weight and BMI but with supraphysiological *r*GWG. A recent study reported higher nitrite/nitrate ratio level, suggestive of higher NO generation, in human placenta homogenates from women with PGMO compared with normal pre-pregnancy BMI [37]. Unfortunately, NO generation in the placenta was determined in the absence of a NOS

inhibitor [37]. In the present study, PGMO associated with lower L-NAME–inhibited (i.e., NOS activity) NO level and L-citrulline generation compared with PGMN.

The amino acid L-arginine is the substrate for NOS to synthesise NO [38]. In HUVECs, L-arginine uptake is mediated mainly via the human cationic amino acid transporters (hCATs) and system y^+L activity [22,39–41]. L-Arginine uptake via these membrane transporters is required for eNOS activity in HUVECs [40,41]. PGMO associated with higher maximal L-arginine transport capacity (V_{max}/K_m) and expression of the hCATs isoform 1 (hCAT-1) in HUVECs. Since L-arginine transport was increased but NOS activity was reduced in PGMO the increased transport may result in response to the reduced NO synthesis seen in HUVECs. This phenomenon was also suggested for HUVECs from women with supraphysiological *r*GWG [12], preeclampsia [42], and in response to ER stress [43]. Also, since intracellular L-arginine is a substrate for arginases in HUVECs [29], and arginase activity was higher in these cells from PGMO, it is likely that these enzymes will preferentially metabolise this amino acid limiting its availability to eNOS in this cell type [44]. Since the apparent K_m for L-arginine transport was in the range of hCAT-1 described for this cell type (~100-200 μmol/L) [40,41], the saturable transport fitted to a single first order lineal regression in Eadie-Hofstee plots (suggestive of a single membrane transport mechanism or more than one mechanism with similar K_m) [45], and PGMO increased the hCAT-1 protein abundance, increased in hCAT-1 expression and activity may explain the higher L-arginine transport in HUVECs from PGMO compared with PGMN pregnancies is likely.

4.2 ER stress in PGMO

ER stress is induced in HUVECs exposed to the lipid peroxidation product 4-hydroxy-trans-2-nonenal [46]. Also, activation of the unfolded protein response (UPR) initiators PERK, IRE1, and ATF6 is reported in human antecubital vein endothelial cells from obese subjects [13]. Interestingly, ER stress associates with endothelial dysfunction by reducing eNOS activation [16,18,47] via still unclear mechanisms [9]. Since HUVECs from PGMO express high levels of these UPR markers, suggest that PGMO results in ER stress in this cell type. PGMO associated with a higher phosphorylation of PERK at Thr^{981} suggesting PERK activation as reported in HUVECs exposed to lipid peroxidation products [46] and endothelial cells from obese subjects [13]. Interestingly, PERK activation associated with eNOS uncoupling due to an endoplasmic reticulum redox imbalance-induced dissociation of HSP90 to eNOS in HUVECs [48]. This phenomenon resulted in lower activator Ser^{1177} phosphorylation at eNOS. Thus, PGMO reduced eNOS phosphorylation at Ser^{1177} may result from PERK activation in HUVECs. Interestingly, PGMO-increased PERK activation was unaltered by the ER stress inducer tunicamycin [23], suggesting that obesity effect altering this parameter may be maximal. The latter is supported by the findings showing that tunicamycin increased PERK phosphorylation up to a comparable level as seen in cells from PGMN. The possibility that PGMO results in ER stress in HUVECs is also supported by the results showing that TUDCA, a reducer of ER stress [24], blocked the effect of PGMO and tunicamycin on PERK phosphorylation.

PERK activation results in eIF2α phosphorylation, leading to lower general translation but higher translation of several proteins [43]. eIF2α phosphorylation associated with an ATF4-mediated increase in CHOP and CAT-1 expression in mammalian cells [49,50]. Our findings showed that eIF2α phosphorylation, CHOP mRNA expression, and CHOP and hCAT-1 protein abundance were increased in PGMO compared with PGMN.

Since eIF2α phosphorylation results in hCAT-1 increased expression in mouse embryonic fibroblasts [51,52], PGMO-increased L-arginine transport may result from an inhibitory phosphorylation of eIF2α. Also, expression of TRB3, a CHOP-mediated inducible gene in ER stress [53], was higher in cells from PGMO. TRB3 is a protein linking ER stress and endothelial dysfunction since acts as a pseudokinase blocking Akt activity [54,55], one of the main eNOS activators causing its phosphorylation on Ser^{1177} [9,38]. Since PGMO associated with lower Akt activator phosphorylation and this effect was reversed by TUDCA, PGMO-increased TRB3 level may also involve Akt inactivation. Thus, higher TRB3 protein abundance could reduce eNOS activity in HUVECs from PGMO. Changes in eIF2α, CHOP, and TRB3 expression were unaltered by tunicamycin but blocked by TUDCA in PGMO. Thus, the increase in PERK–eIF2α–CHOP–TRB3 axis suggests that PGMO results in increased ER stress in the foetoplacental endothelium. This phenomenon ends in lower eNOS activity in HUVECs from PGMO by still unveiled mechanisms.

Increased CHOP protein abundance and activity downregulates the expression of plasma membrane transporters including the human equilibrative nucleoside transporter 1 (hENT1) in HUVECs [56]. In HUVECs from gestational diabetes mellitus, increased CHOP activity reduces hENT1 expression and its V_{max}/K_m for adenosine transport. Since a higher V_{max}/K_m for L-arginine was found in cells from PGMO as well as in cells from PGMN exposed to tunicamycin, a CHOP-mediated increase in the expression of hCAT-1 in HUVECs is likely. The possibility that PERK–eIF2α–CHOP–TRB3 axis is responsible for the PGMO-increased hCAT-1–mediated L-arginine transport is supported by the fact that the increase in PERK (~2 fold) and eIF2α (~2.6 fold) phosphorylation, and CHOP (~2.3 fold) and TRB3 (~1.8 fold) protein abundances were similar to the increase seen in the

V_{max}/K_m for L-arginine (~1.6 fold) in cells from this condition. Reports in HUVECs and other endothelial cells show that PERK [48], eIF2α [57], CHOP [57] and TRB3 [58] inhibit eNOS. Also, changes in the expression and phosphorylation of these ER stress markers were similar to the increase in the inhibitor Thr^{495} phosphorylation of eNOS (~1.7 fold) and reduced NO generation. Thus, PERK–eIF2α–CHOP–TRB3 axis activation lowers eNOS activity in HUVECs from PGMO pregnancies.

IRE-1α is also part of the ER stress response in mammalian cells [50,59]. A redox imbalance-induced ER stress in HUVECs causes IRE-1α dissociation from HSP90 leading to uncoupled eNOS and lower NO generation [48]. Also, increased IRE-1α expression and phosphorylation associated with lower eNOS activity in placental tissues from preeclampsia [57]. Since IRE-1α protein abundance, but not its phosphorylation, was increased in cells from PGMO (~1.8 fold) compared with PGMN, whether IRE-1α participates in the PGMO-reduced eNOS activity is uncertain. However, since tunicamycin did not alter but TUDCA blocked the effect of PGMO on IRE-1α protein abundance, and because endothelial cells from obese subjects show increased IRE-1α protein abundance [13] and placental tissue extracts from preeclampsia show a parallel increase in IRE-1α protein abundance and phosphorylation [57], PGMO deleterious consequences for eNOS activity may result from increased protein abundance rather than changes in the phosphorylation of this ER stress marker.

IRE-1α causes splicing of XBP-1 in several cell types [50,59]. Redox imbalance-induced ER stress associated with XBP-1 splicing in HUVECs [46] and increased XBP-1 expression in placental tissue [57]. However, HUVECs from PGMO show not changes in XBP1 mRNA expression and similar splicing in response to tunicamycin than cells from

PGMN. Thus, PGMO-induced ER stress may not involve an IRE-1α–mediated response in HUVECs. Interestingly, increased IRE-1α protein abundance associated with a comparable increase in JNK1 phosphorylation in cells from PGMO. JNK1 is a kinase activated directly by the IRE1α kinase domain [60,61]. JNK1 activation results in defective insulin signalling due to reduced activation of insulin receptor substrate 1 in HUVECs [9,62]. PGMO associates with insulin resistance [63] suggesting that ER stress induced by this maternal condition may result in increased IRE-1α–JNK1 axis signalling in HUVECs limiting their reactivity to insulin. This possibility is supported by the results showing that TUDCA inhibits the PGMO-associated increase in JNK1 phosphorylation. Also, cells from PGMN pregnancies show higher JNK1 phosphorylation in response to tunicamycin, a response blocked by TUDCA, suggesting that ER stress increases JNK1 also in cells from PGMN pregnancies.

A preferential nuclear localization of ATF6 is considered a marker of ER stress [13,50,59], as reported in HUVECs [64]. Also, antecubital endothelial cells from obese subjects show increased ATF6 nuclear localization compared with non-obese subjects [13]. Since HUVECs from PGMO show preferential ATF6 nuclear localization compared with cells from PGMN, and this phenomenon was blocked by TUDCA but unaltered by tunicamycin, PGMO induced ATF6-associated ER stress in HUVECs.

In summary, HUVECs from women with PGMO show reduced eNOS activity with increased hCAT-1–mediated L-arginine transport as a potential compensatory mechanism (Fig. 6). HUVECs from PGMO pregnancies show UPR activation compared with cells from PGMN pregnancies. UPR activation results in higher expression of the PERK–eIF2α–CHOP–TRB3 axis signalling, with less clear changes in IRE1α–XBP1 axis signalling. UPR

activation also resulted in higher nuclear localization of ATF6. Since the changes seen in PERK–eIF2α–CHOP–TRB3 are similar to the inhibitory phosphorylation of eNOS at Thr^{495} and reduced NO levels, and the potential redistribution of ATF6 in the cell, we suggest that PGMO is a condition causing ER stress leading to foetoplacental endothelial dysfunction. It is worth mentioning that a different maternal metabolic state during pregnancy which could be caused by either PGMO or the pregnancy itself may also result in altering the parameters described in this study. Also, changes seen *in vitro* may result as an adaptation to culture and not necessarily reflecting a similar situation *in vivo*. Pre-pregnancy obesity is a deleterious condition leading to an abnormal newborn phenotype that could have serious consequences in its adulthood. Interestingly, TUDCA mitigates ER stress-associated endothelial dysfunction in young humans that were subjected to an oral glucose load [65], and incubation of HUVECs from normal pregnancies with plasma from children with pre-pubertal obesity caused a lower NO synthesis in response to insulin involving ER stress [66]. Also, administration of TUDCA increased the response of patients with amyotrophic lateral sclerosis to the Amyotrophic Lateral Sclerosis Functional Rating Scale Revised test, making likely that ER stress could be a factor involved in the subjects with this disease [67]. Even when the latter study did not address whether TUDCA effect was due to reducing a potential ER stress in these subjects, it is noticeable to consider that these approaches show that using ER stress blockers in humans is safe. Unfortunately, nothing has been reported *in vivo* in human subjects regarding pregnant women with PGMO. Considering these findings *in vivo* we speculate on the possibility that a proper management of the ER stress condition in the mother with PGMO may result in a better newborn outcome from these pregnancies.

Conflict of interest

The authors confirm that there are no conflicts of interest.

Sources of funding

This work was supported by the Fondo Nacional de Desarrollo Científico y Tecnológico (FONDECYT) [grant numbers 1150377, 1121145, 11150083] and Servicio de Salud de Medicina Oriente, Hospital San Juan de Dios [Res. 1938-2016], Santiago, Chile. RV-L, MS, and LSi hold PhD fellowships from the Comisión Nacional para la Investigación en Ciencia y Tecnología (CONICYT) (Chile), and ViceRectorate of Research, PUC (Chile). LSi holds a PhD fellowship from The Abel Tasman Talent Program and University Medical Center Groningen (UMCG) (The Netherlands).

Disclosures

None.

References

[1] World Health Organization (WHO), Obesity and Overweight. Fact sheet 311, World Health Organization Geneva, Switzerland (2018), http://www.who.int/mediacentre/factsheets/fs311/en/.

[2] J. Pirkola, A. Pouta, A. Bloigu, A.L. Hartikainen, J. Laitinen, M.R. Järvelin, M. Vääräsmäki, Risks of overweight and abdominal obesity at age 16 years associated with prenatal exposures to maternal prepregnancy overweight and gestational diabetes mellitus, Diabetes Care 33 (2010) 1115–1121, http://dx.doi.org/10.2337/dc09-1871.

[3] R. Gaillard, E.A.P. Steegers, L. Duijts, J.F. Felix, A. Hofman, O.H. Franco, V.W.V Jaddoe, Childhood cardiometabolic outcomes of maternal obesity during pregnancy: The generation R study, Hypertension 63 (2014) 683–691, http://dx.doi.org/10.1161/HYPERTENSIONAHA.113.02671.

[4] A.A. Mamun, M. O'Callaghan, L. Callaway, G. Williams, J. Najman, D.A. Lawlor, Associations of gestational weight gain with offspring body mass index and blood pressure at 21 years of age evidence from a birth cohort study, Circulation 119 (2009) 1720–1727, http://dx.doi.org/10.1161/CIRCULATIONAHA.108.813436.

[5] V.H.J. Roberts, A.E. Frias, K.L. Grove, Impact of maternal obesity on fetal programming of cardiovascular disease, Physiology (Bethesda) 30 (2015) 224–231, http://dx.doi.org/10.1152/physiol.00021.2014.

[6] N.C. Penfold, S.E. Ozanne, Developmental programming by maternal obesity in 2015: Outcomes, mechanisms, and potential interventions, Horm. Behav. 76 (2015) 143–152, http://dx.doi.org/10.1016/j.yhbeh.2015.06.015.

[7] F. Pardo, R. Villalobos-Labra, B. Sobrevia, F. Toledo, L. Sobrevia, Extracellular vesicles in obesity and diabetes mellitus, Mol. Aspects Med. 60 (2018) 81–91, http://dx.doi.org/10.1016/j.mam.2017.11.010.

[8] F. Pardo, R. Villalobos-Labra, D.I. Chiarello, R. Salsoso, F. Toledo, J. Gutierrez, A. Leiva, L. Sobrevia, Molecular implications of adenosine in obesity, Mol. Aspects Med. 55 (2017) 90–101, http://dx.doi.org/10.1016/j.mam.2017.01.003.

[9] R. Villalobos-Labra, L. Silva, M. Subiabre, J. Araos, R. Salsoso, B. Fuenzalida, T. Sáez, F. Toledo, M. González, C. Quezada, F. Pardo, D.I. Chiarello, A. Leiva, L. Sobrevia, Akt/mTOR role in human foetoplacental vascular insulin resistance in diseases of pregnancy, J. Diabetes Res. 2017 (2017) 1–13, http://dx.doi.org/10.1155/2017/5947859.

[10] D. Versari, E. Daghini, A. Virdis, L. Ghiadoni, S. Taddei, Endothelial dysfunction as a target for prevention of cardiovascular disease, Diabetes Care. 32 Suppl 2 (2009) S314–S321, http://dx.doi.org/10.2337/dc09-S330.

[11] L. Sarno, G.M. Maruotti, G. Saccone, M. Morlando, A. Sirico, P. Martinelli, Maternal body mass index influences umbilical artery Doppler velocimetry in physiologic pregnancies, Prenat. Diagn. 35 (2015) 125–128, http://dx.doi.org/10.1002/pd.4499.

[12] F. Pardo, L. Silva, T. Sáez, R. Salsoso, J. Gutiérrez, C. Sanhueza, A. Leiva, L. Sobrevia, Human supraphysiological gestational weight gain and fetoplacental vascular dysfunction, Int. J. Obes. 39 (2015) 1264–1273, http://dx.doi.org/10.1038/ijo.2015.57.

[13] R.E. Kaplon, E. Chung, L. Reese, K. Cox-York, D.R. Seals, C.L. Gentile, Activation of the unfolded protein response in vascular endothelial cells of

nondiabetic obese adults, J. Clin. Endocrinol. Metab. 98 (2013) E1505-E1509, http://dx.doi.org/10.1210/jc.2013-1841.

[14] M. Flamment, E. Hajduch, P. Ferré, F. Foufelle, New insights into ER stress-induced insulin resistance, Trends Endocrinol. Metab. 23 (2012) 381–390, http://dx.doi.org/10.1016/j.tem.2012.06.003.

[15] Y.M. Taalab, N. Ibrahim, A. Maher, M. Hassan, W. Mohamed, A.A. Moustafa, M. Salama, D. Johar, L. Bernstein, Mechanisms of disordered neurodegenerative function: Concepts and facts about the different roles of the protein kinase RNA-like endoplasmic reticulum kinase (PERK), Rev. Neurosci. (2018), http://dx.doi.org/10.1515/revneuro-2017-0071.

[16] D. Murugan, Y.S. Lau, W.C. Lau, M.R. Mustafa, Y. Huang, Angiotensin 1-7 protects against angiotensin II-induced endoplasmic reticulum stress and endothelial dysfunction via mas receptor, PLoS One 10 (2015), http://dx.doi.org/10.1371/journal.pone.0145413.

[17] J. Kim, H.J. Jang, D.H. Hwang, Toll-like receptor 4-induced endoplasmic reticulum stress contributes to impairment of vasodilator action of insulin, Am. J. Physiol. 309 (2015) E767–E776, http://dx.doi.org/10.1152/ajpendo.00369.2015.

[18] M. Galán, M. Kassan, P.J. Kadowitz, M. Trebak, S. Belmadani, K. Matrougui, Mechanism of endoplasmic reticulum stress-induced vascular endothelial dysfunction, Biochim. Biophys. Acta - Mol. Cell Res. 1843 (2014) 1063–1075, http://dx.doi.org/10.1016/j.bbamcr.2014.02.009.

[19] S. Liong, M. Lappas, Endoplasmic reticulum stress regulates inflammation and insulin resistance in skeletal muscle from pregnant women, Mol. Cell. Endocrinol. 425 (2016) 11–25, http://dx.doi.org/10.1016/j.mce.2016.02.016.

[20] K.M. Rasmussen, A.L. Yaktine, I. of M. (US) and N.R.C. Guidelines, (US) Committee to Reexamine IOM Pregnancy Weight, Weight Gain During Pregnancy, National Academies Press (US), 2009, http://dx.doi.org/10.17226/12584.

[21] Ministerio de Salud (MINSAL), Guía perinatal 2015, Gobierno de Chile (2015).

[22] M. Subiabre, L. Silva, R. Villalobos-Labra, F. Toledo, M. Paublo, M.A. López, R. Salsoso, F. Pardo, A. Leiva, L. Sobrevia, Maternal insulin therapy does not restore foetoplacental endothelial dysfunction in gestational diabetes mellitus, Biochim. Biophys. Acta - Mol. Basis Dis. 1863 (2017) 2987–2998, http://dx.doi.org/10.1016/j.bbadis.2017.07.022.

[23] C.M. Oslowski, F. Urano, Measuring ER stress and the unfolded protein response using mammalian tissue culture system, Methods Enzymol. 490 (2011) 71–92, http://dx.doi.org/10.1016/B978-0-12-385114-7.00004-0.

[24] Y.M. Yoon, J.H. Lee, S.P. Yun, Y.S. Han, C.W. Yun, H.J. Lee, H. Noh, S.J. Lee, H.J. Han, S.H. Lee, Tauroursodeoxycholic acid reduces ER stress by regulating of Akt-dependent cellular prion protein, Sci. Rep. 6 (2016) 39838, http://dx.doi.org/10.1038/srep39838.

[25] I. Fleming, R. Busse, Molecular mechanisms involved in the regulation of the endothelial nitric oxide synthase, Am. J. Physiol. 284 (2003) R1–R12, http://dx.doi.org/10.1152/ajpregu.00323.2002.

[26] E. Guzmán-Gutiérrez, A. Armella, F. Toledo, F. Pardo, A. Leiva, L. Sobrevia, Insulin requires A1 adenosine receptors expression to reverse gestational diabetes-increased L-arginine transport in human umbilical vein endothelium, Purinergic Signal. 12 (2016) 175–190, http://dx.doi.org/10.1007/s11302-015-9491-2.

[27] J. Antonov, D.R. Goldstein, A. Oberli, A. Baltzer, M. Pirotta, A. Fleischmann, H.J. Altermatt, R. Jaggi, Reliable gene expression measurements from degraded RNA by quantitative real-time PCR depend on short amplicons and a proper normalization, Lab. Investig. 85 (2005) 1040–1050, http://dx.doi.org/10.1038/labinvest.3700303.

[28] A. Uemura, M. Oku, K. Mori, H. Yoshida, Unconventional splicing of XBP1 mRNA occurs in the cytoplasm during the mammalian unfolded protein response, J. Cell Sci. 122 (2009) 2877–2886, http://dx.doi.org/10.1242/jcs.040584.

[29] C.P. Prieto, B.J. Krause, C. Quezada, R. San Martín, L. Sobrevia, P. Casanello, Hypoxia-reduced nitric oxide synthase activity is partially explained by higher arginase-2 activity and cellular redistribution in human umbilical vein endothelium, Placenta 32 (2011) 932–940, http://dx.doi.org/10.1016/j.placenta.2011.09.003.

[30] N.N. Kim, J.D. Cox, R.F. Baggio, F.A. Emig, S.K. Mistry, S.L. Harper, D.W. Speicher, S.M.Jr. Morris, D.E. Ash, A. Traish, D.W. Christianson, Probing erectile function: S-(2-boronoethyl)-L-cysteine binds to arginase as a transition state analogue and enhances smooth muscle relaxation in human penile corpus cavernosum, Biochemistry 40 (2001) 2678–2688, http://dx.doi.org/10.1021/bi002317h.

[31] P.J. Sáez, K.F. Shoji, M.A. Retamal, P.A. Harcha, G. Ramírez, J.X. Jiang, R. von Bernhardi, J.C. Sáez, ATP is required and advances cytokine-induced gap junction formation in microglia in vitro, Mediators Inflamm. 2013 (2013) 216402, http://dx.doi.org/10.1155/2013/216402.

[32] J. Schindelin, I. Arganda-Carreras, E. Frise, V. Kaynig, M. Longair, T. Pietzsch, S. Preibisch, C. Rueden, S. Saalfeld, B. Schmid, J.Y. Tinevez, D.J. White, V. Hartenstein, K. Eliceiri, P. Tomancak, A. Cardona, Fiji: an open-source platform for

biological-image analysis, Nat Methods 9 (2012) 676–682, http://dx.doi.org/10.1038/nmeth.2019

[33] L. Iaffaldano, C. Nardelli, F. D'Alessio, V. D'Argenio, M. Nunziato, L. Mauriello, C. Procaccini, G.M. Maruotti, P. Martinelli, G. Matarese, L. Pastore, L. Del Vecchio, G. Labruna, L. Sacchetti, Altered bioenergetic profile in umbilical cord and amniotic mesenchymal stem cells from newborns of obese women, Stem Cells Dev. 27 (2018) 199–206, http://dx.doi.org/10.1089/scd.2017.0198.

[34] K. Mitsuya, A.N. Parker, L. Liu, J. Ruan, M.C.M. Vissers, L. Myatt, Alterations in the placental methylome with maternal obesity and evidence for metabolic regulation, PLoS One 12 (2017) e0186115, http://dx.doi.org/10.1371/ journal.pone.0186115.

[35] M. Kovo, E. Zion-Saukhanov, L. Schreiber, N. Mevorach, M. Divon, A. Ben-Haroush, J. Bar, The effect of maternal obesity on pregnancy outcome in correlation with placental pathology, Reprod. Sci. 22 (2015) 1643–1648, http://dx.doi.org/10.1177/1933719115592712.

[36] P. Di Fulvio, A. Pandolfi, G. Formoso, S. Di Silvestre, P. Di Tomo, A. Giardinelli, A. De Marco, N. Di Pietro, M. Taraborrelli, S. Sancilio, R. Di Pietro, M. Piantelli, A. Consoli, Features of endothelial dysfunction in umbilical cord vessels of women with gestational diabetes, Nutr. Metab. Cardiovasc. Dis. 24 (2014) 1337–1345, http://dx.doi.org/ 10.1016/j.numecd.2014.06.005.

[37] L. Evans, L. Myatt, Sexual dimorphism in the effect of maternal obesity on antioxidant defence mechanisms in the human placenta, Placenta 51 (2017) 64–69, http://dx.doi.org/10.1016/j.placenta.2017.02.004.

[38] I. Fleming, Molecular mechanisms underlying the activation of eNOS, Pflugers Arch. 459 (2010) 793–806, http://dx.doi.org/10.1007/s00424-009-0767-7.

[39] Y. Arancibia-Garavilla, F. Toledo, P. Casanello, L. Sobrevia, Nitric oxide synthesis requires activity of the cationic and neutral amino acid transport system y+L in human umbilical vein endothelium, Exp. Physiol. 88 (2003) 699–710, http://dx.doi.org/10.1113/eph8802647.

[40] T. Sáez, R. Salsoso, A. Leiva, F. Toledo, P. de Vos, M. Faas, L. Sobrevia, Human umbilical vein endothelium-derived exosomes play a role in foetoplacental endothelial dysfunction in gestational diabetes mellitus, Biochim. Biophys. Acta - Mol. Basis Dis. 1864 (2018) 499–508, http://dx.doi.org/10.1016/j.bbadis.2017.11.010.

[41] M.A. Ramírez, J. Morales, M. Cornejo, E.H. Blanco, E. Mancilla-Sierpe, F. Toledo, A.R. Beltrán, L. Sobrevia, Intracellular acidification reduces L-arginine transport via system y+L but not via system y+/CATs and nitric oxide synthase activity in human umbilical vein endothelial cells, Biochim. Biophys. Acta - Mol. Basis Dis. 1864 (2018) 1192–1202, http://dx.doi.org/10.1016/j.bbadis.2018.01.032.

[42] R. Salsoso, E. Guzmán-Gutiérrez, T. Sáez, K. Bugueño, M.A. Ramírez, M. Farías, F. Pardo, A. Leiva, C. Sanhueza, A. Mate, C. Vázquez, L. Sobrevia, Insulin restores L-arginine transport requiring adenosine receptors activation in umbilical vein endothelium from late-onset preeclampsia, Placenta 36 (2015) 287–296, http://dx.doi.org/10.1016/j.placenta.2014.12.007.

[43] A.A. Komar, M. Hatzoglou, Cellular IRES-mediated translation: The war of ITAFs in pathophysiological states, Cell Cycle 10 (2011) 229–240, http://dx.doi.org/10.4161/cc.10.2.14472.

[44] A. Leiva, C.D. De Medina, R. Salsoso, T. Sáez, S. San Martín, F. Abarzúa, M. Farías, E. Guzmán-Gutiérrez, F. Pardo, L. Sobrevia, Maternal hypercholesterolemia in pregnancy associates with umbilical vein endothelial dysfunction: Role of endothelial nitric oxide synthase and arginase II, Arterioscler. Thromb. Vasc. Biol. 33 (2013) 2444–2453. http://dx.doi.org/10.1161/ATVBAHA.113.301987.

[45] R. Devés, C.A.R. Boyd, Transporters for cationic amino acids in animal cells: Discovery, structure, and function, Physiol. Rev. 78 (1998) 487–545, http://dx.doi.org/10.1016/0022-4804(91)90210-D.

[46] E. Vladykovskaya, S.D. Sithu, P. Haberzettl, N.S. Wickramasinghe, M.L. Merchant, B.G. Hill, J. McCracken, A. Agarwal, S. Dougherty, S.A. Gordon, D.A. Schuschke, O.A. Barski, T. O'Toole, S.E. D'Souza, A. Bhatnagar, S. Srivastava, Lipid peroxidation product 4-hydroxy-trans-2-nonenal causes endothelial activation by inducing endoplasmic reticulum stress, J. Biol. Chem. 287 (2012) 11398–11409, http://dx.doi.org/10.1074/jbc.M111.320416.

[47] W.S. Cheang, X.Y. Tian, W.T. Wong, C.W. Lau, S.S.T. Lee, Z.Y. Chen, X. Yao, N. Wang, Y. Huang, Metformin protects endothelial function in diet-induced obese mice by inhibition of endoplasmic reticulum stress through 5' adenosine monophosphate-activated protein kinase-peroxisome proliferator-activated receptor δ pathway, Arterioscler. Thromb. Vasc. Biol. 34 (2014) 830–836, http://dx.doi.org/10.1161/ATVBAHA.113.301938.

[48] H.Y. Lee, H. Maher, A. Zeeshan, H.R. Kim, H.J. Chae, Nox4 regulates the eNOS uncoupling process in aging endothelial cells, Free Radic. Biol. Med. 113 (2017) 26–35, http://dx.doi.org/10.1016/j.freeradbiomed.2017.09.010.

[49] M.S. Kilberg, J. Shan, N. Su, ATF4-dependent transcription mediates signaling of amino acid limitation, Trends Endocrinol. Metab. 20 (2009) 436–443, http://dx.doi.org/10.1016/j.tem.2009.05.008.

[50] J. Grootjans, A. Kaser, R.J. Kaufman, R.S. Blumberg, The unfolded protein response in immunity and inflammation, Nat. Rev. Immunol. 16 (2016) 469–484, http://dx.doi.org/10.1038/nri.2016.62.

[51] A.B. Lopez, C. Wang, C.C. Huang, I. Yaman, Y. Li, K. Chakravarty, P.F. Johnson, C.M. Chiang, M.D. Snider, R.C. Wek, M. Hatzoglou, A feedback transcriptional mechanism controls the level of the arginine/lysine transporter CAT-1 during amino acid starvation, Biochem J. 402 (2007) 163–173, http://dx.doi.org/10.1042/BJ20060941.

[52] C.C. Huang, Y. Li, A.B. Lopez, C.M. Chiang, R.J. Kaufman, M.D. Snider, M. Hatzoglou, C. Huang, A. Lopez, Temporal regulation of Cat-1 (cationic amino acid transporter-1) gene transcription during endoplasmic reticulum stress, Biochem J. 1 (2010) 215–224, http://dx.doi.org/10.1042/BJ20100286.

[53] N. Ohoka, S. Yoshii, T. Hattori, K. Onozaki, H. Hayashi, TRB3, a novel ER stress-inducible gene, is induced via ATF4-CHOP pathway and is involved in cell death, EMBO J. 24 (2005) 1243–1255, http://dx.doi.org/10.1038/sj.emboj.7600596.

[54] K. Du, S. Herzig, R.N. Kulkarni, M. Montminy, TRB3: a tribbles homolog that inhibits Akt/PKB activation by insulin in liver, Science 300 (2003) 1574–1577, http://dx.doi.org/10.1126/science.1079817.

[55] R. Marinho, R.A. Mekary, V.R. Muñoz, R.J. Gomes, J.R. Pauli, L.P. de Moura, Regulation of hepatic TRB3/Akt interaction induced by physical exercise and its

effect on the hepatic glucose production in an insulin resistance state, Diabetol. Metab. Syndr. 7 (2015) 67, http://dx.doi.org/10.1186/s13098-015-0064-x.

[56] M. Farías, C. Puebla, F. Westermeier, M.J. Jo, M. Pastor-Anglada, P. Casanello, L. Sobrevia, Nitric oxide reduces SLC29A1 promoter activity and adenosine transport involving transcription factor complex hCHOP-C/EBPα in human umbilical vein endothelial cells from gestational diabetes, Cardiovasc. Res. 86 (2010) 45–54, http://dx.doi.org/10.1093/cvr/cvp410.

[57] L. Du, F. He, L. Kuang, W. Tang, Y. Li, D. Chen, eNOS/iNOS and endoplasmic reticulum stress-induced apoptosis in the placentas of patients with preeclampsia, J. Hum. Hypertens. 31 (2017) 49–55, http://dx.doi.org/10.1038/jhh.2016.17.

[58] P. Abeyrathna, Y. Su, The critical role of Akt in cardiovascular function, Vascul. Pharmacol. 74 (2015) 38–48, http://dx.doi.org/10.1016/j.vph.2015.05.008.

[59] E. Dufey, D. Sepúlveda, D. Rojas-Rivera, C. Hetz, Cellular mechanisms of endoplasmic reticulum stress signaling in health and disease. 1. An overview, Am. J. Physiol. Cell Physiol. 307 (2014) C582-C594, http://dx.doi.org/10.1152/ajpcell.00258.2014.

[60] F. Urano, X. Wang, A. Bertolotti, Y. Zhang, P. Chung, H.P. Harding, D. Ron, Coupling of stress in the ER to activation of JNK protein kinases by transmembrane protein kinase IRE1, Science 287 (2000) 664–666, http://dx.doi.org/10.1126/science.287.5453.664.

[61] U. Ozcan, Q. Cao, E. Yilmaz, A.H. Lee, N.N. Iwakoshi, E. Ozdelen, G. Tuncman, C. Görgün, L.H. Glimcher, G.S. Hotamisligil, Endoplasmic reticulum stress links obesity, insulin action, and type 2 diabetes, Science 306 (2004) 457–461, http://dx.doi.org/10.1126/science.1103160.

[62] V. De Nigris, G. Pujadas, L. La Sala, R. Testa, S. Genovese, A. Ceriello, Short-term high glucose exposure impairs insulin signaling in endothelial cells, Cardiovasc. Diabetol. 14 (2015) 114, http://dx.doi.org/10.1186/s12933-015-0278-0.

[63] G. Carreras-Badosa, A. Bonmatí, F.J. Ortega, J.M. Mercader, M. Guindo-Martínez, D. Torrents, A. Prats-Puig, J.M. Martinez-Calcerrada, E. Platero-Gutierrez, F. De Zegher, L. Ibáñez, J.M. Fernandez-Real, A. Lopez-Bermejo, J. Bassols, Altered circulating miRNA expression profile in pregestational and gestational obesity, J. Clin. Endocrinol. Metab. 100 (2015) E1446–E1456, http://dx.doi.org/10.1210/jc.2015-2872.

[64] Q. Su, Y. Wang, X. Yang, X.D. Li, Y.F. Qi, X.J. He, Y.J. Wang, Inhibition of endoplasmic reticulum stress apoptosis by estrogen protects human umbilical vein endothelial cells through the PI3 kinase-Akt signaling pathway, J. Cell. Biochem. 118 (2017) 4568–4574, http://dx.doi.org/10.1002/jcb.26120.

[65] L.K. Walsh, R.M. Restaino, M. Neuringer, C. Manrique, J. Padilla, Administration of tauroursodeoxycholic acid prevents endothelial dysfunction caused by an oral glucose load, Clin. Sci. (Lond). 130 (2016) 1881–1888, http://dx.doi.org/10.1042/CS20160501.

[66] N. Di Pietro, M.L. Marcovecchio, S. Di Silvestre, T. de Giorgis, V.G.P. Cordone, P. Lanuti, F. Chiarelli, G. Bologna, A. Mohn, A. Pandolfi, Plasma from pre-pubertal obese children impairs insulin stimulated Nitric Oxide (NO) bioavailability in endothelial cells: Role of ER stress, Mol. Cell. Endocrinol. 443 (2017) 52–62, doi: http://dx.doi.org/10.1016/j.mce.2017.01.001.

[67] A.E. Elia, S. Lalli, M.R. Monsurrò, A. Sagnelli, A.C. Taiello, B. Reggiori, V. La Bella, G. Tedeschi, A. Albanese, Tauroursodeoxycholic acid in the treatment of

patients with amyotrophic lateral sclerosis, Eur. J. Neurol. 23 (2016) 45–52, doi: http://dx.doi.org/10.1111/ene.12664.

Figure 1. Involvement of endoplasmic reticulum stress in L-arginine transport in HUVECs. Endothelial cells were isolated from umbilical veins where pregnant women were with a normal pre-pregnancy body mass index (PGMN, *n* = 12 different women) or with pre-pregnancy obesity (PGMO, *n* = 12 different women). Cells were exposed (8 h) to culture medium without (Control) or with tunicamycin (5 μmol/L, inducer of endoplasmic reticulum stress), tauroursodeoxycholic acid (TUDCA, 100 μmol/L, reducer of endoplasmic reticulum stress), or both (see Materials and methods). A and B. Overall transport of L-arginine (0–1000 μmol/L L-arginine, 1 min, 37°C) was fitted to a single Michaelis-Menten equation increased in a linear component and represented in Eadie-Hofstee plots (*lower panels*). C and D. Saturable transport of L-arginine derived by subtracting the nonsaturable, linear component of transport in the range of L-arginine concentrations used in this study from the overall transport (see Materials and methods). Data was fitted to a single Michaelis-Menten equation and represented in Eadie-Hofstee plots (*lower panels*). E. Western blot (representative of nine experiments) for human cationic amino acid transporter 1 (hCAT-1) protein abundance in HUVECs from PGMN (*n* = 9 different women) or PGMO (*n* = 9 different women). The graph shows hCAT-1/β-actin ratio densitometries normalized to 1 in Control in PGMN. In E, **P*<0.05 versus Control in PGMN, †*P*<0.05 versus Control and tunicamycin in PGMO, § and ‡ *P*<0.05 versus tunicamycin in PGMN and PGMO, respectively. Values are mean ± S.E.M..

Figure 2. Involvement of endoplasmic reticulum stress in eNOS expression and activity and arginase activity in HUVECs. Endothelial cells were isolated from umbilical veins where pregnant women were with a normal pre-pregnancy body mass index (PGMN, *n* = 9 different women) or with pre-pregnancy obesity (PGMO, *n* = 9 different women). Cells were exposed (8 h) to culture medium without (Control) or with tunicamycin (5 μmol/L, inducer of endoplasmic reticulum stress), tauroursodeoxycholic acid (TUDCA, 100 μmol/L, reducer of endoplasmic reticulum stress), or both (see Materials and methods). A. Nitric oxide (NO) level detected as relative fluorescence units (RFU) measured in cells from PGMN (*n* = 9 different women) and PGMO (*n* = 9 different women) preloaded with the fluorescent dye 4-amino-5-methylamino-2′,7′-difluorescein (DAF-FM, 5 μmol/L) in the absence or presence of N^G-nitro-L-arginine methyl ester (L-NAME, 100 μmol/L, NO synthase (NOS) inhibitor). *Lower panel*: Fraction of NO level inhibited by L-NAME (i.e., NOS-activity dependent) normalized to 1 in Control in PGMN derived from data in the upper panel. B. L-Citrulline content measured by h.p.l.c. in cells from PGMN (*n* = 3 different women) and PGMO (*n* = 3 different women) in the absence or presence of L-NAME (100 μmol/L) as in A. *Lower panel*: Fraction of L-citrulline content inhibited by L-NAME (i.e., NOS-activity dependent) derived from data in the upper panel. C. Western blot (representative of nine experiments) for total eNOS (Total eNOS) (*upper panel*), eNOS phosphorylated at serine^{1177} (P~Ser^{1177}-eNOS) (*middle panel*) or threonine^{495} (P~Thr^{495}-eNOS) (*lower panel*), and β-actin (internal reference) protein abundance in HUVECs from PGMN (*n* = 9 different women) or PGMO (*n* = 9 different women) as in A. The graphs show Total eNOS/β-actin,

P~Ser^{1177}-eNOS/Total eNOS, or P~Thr^{495}-eNOS/Total eNOS ratio densitometries normalized to 1 in Control in PGMN. D. Western blot (representative of nine experiments) for total Akt (Total Akt), Akt phosphorylated at serine^{473} (P~Ser^{473}-Akt), and β-actin (internal reference) protein abundance in HUVECs from PGMN (n = 9 different women) or PGMO (n = 9 different women) as in A. The graphs show Total Akt/β-actin (*upper panel*) and P~Ser^{1177}-Akt/Total Akt (*lower panel*) ratio densitometries normalized to 1 in Control in PGMN. E. Urea formation measured by colorimetry in cells from PGMN (n = 3 different women) and PGMO (n = 3 different women) in the absence or presence of *S*-(2-boronoethyl)-L-cysteine (BEC, 20 μmol/L, arginases inhibitor) as in A. *Lower panel*: Fraction of urea formation inhibited by BEC (i.e., arginase-activity dependent) derived from data in the upper panel. *P<0.05 versus Control in PGMN, †P<0.05 versus Control and tunicamycin in PGMO, § and ‡ P<0.05 versus tunicamycin in PGMN and PGMO, respectively. Values are mean ± S.E.M..

Figure 3. Effect of maternal pre-pregnancy obesity on PERK-associated endoplasmic reticulum stress markers expression in HUVECs. Endothelial cells were isolated from umbilical veins where pregnant women were with a normal pre-pregnancy body mass index (PGMN, *n* = 9 different women) or with pre-pregnancy obesity (PGMO, *n* = 9 different women). Cells were exposed (8 h) to culture medium without (Control) or with tunicamycin (5 μmol/L, inducer of endoplasmic reticulum stress), tauroursodeoxycholic acid (TUDCA, 100 μmol/L, reducer of endoplasmic reticulum stress), or both (see Materials and methods). A. Western blot (representative of nine experiments) for total protein kinase RNA-like endoplasmic reticulum kinase (PERK) (Total PERK), PERK phosphorylated at threonine^{981} (P~Thr^{981}PERK), and β-actin (internal reference) protein abundance in HUVECs from PGMN (*n* = 9 different women) or PGMO (*n* = 9 different women). The graph shows Total PERK/β-actin ratio densitometries normalized to 1 in Control in PGMN. *Lower panel*: P~Thr^{981}-PERK/Total PERK ratio densitometries normalized to 1 in Control in PGMN. B. Western blot (representative of nine experiments) for total eukaryotic initiation factor 2 (Total eIF2α) and eIF2α phosphorylated at serine^{51} (P~Ser^{51}eIF2α) as in A. The graph shows Total eIF2α/β-actin ratio densitometries normalized to 1 in Control in PGMN. *Lower panel*: P~Ser^{51}eIF2α /total eIF2α ratio densitometries normalized to 1 in Control in PGMN. C. Western blot (representative of nine experiments) for total C/EBP homologous protein 10 (CHOP) and tribbles-like protein 3 (TRB3) as in A. The graphs show Total CHOP or TRB3/β-actin ratio densitometries normalized to 1 in Control in PGMN. D. Relative mRNA expression for CHOP (*upper panel*), TRB3 (*middle panel*), or

binding immunoglobulin protein (BIP) (*lower panel*) in HUVECs as in A. **P*<0.05 versus Control in PGMN, †*P*<0.05 versus Control and tunicamycin in PGMO, §*P*<0.05 versus tunicamycin in PGMN. Values are mean ± S.E.M..

Figure 4. Effect of maternal pre-pregnancy obesity on IRE1α-associated endoplasmic reticulum stress markers expression in HUVECs. Endothelial cells were isolated from umbilical veins where pregnant women were with a normal pre-pregnancy body mass index (PGMN, *n* = 8 different women) or with pre-pregnancy obesity (PGMO, *n* = 8 different women). Cells were exposed (8 h) to culture medium without (Control) or with tunicamycin (5 μmol/L, inducer of endoplasmic reticulum stress), tauroursodeoxycholic acid (TUDCA, 100 μmol/L, reducer of endoplasmic reticulum stress), or both (see Materials and methods). A. Western blot (representative of eight experiments) for total inositol-requiring enzyme 1α (Total IRE1α), IRE1α phosphorylated at serine^{724} (P-Ser^{724}IRE1α), and β-actin (internal reference) protein abundance in HUVECs from PGMN (*n* = 8 different women) or PGMO (*n* = 8 different women). The graph shows Total IRE1α/β-actin ratio densitometries normalized to 1 in Control in PGMN. *Lower panel*: P~Ser^{724}IRE1α/Total IRE1α ratio densitometries normalized to 1 in Control in PGMN. B. Level of the unspliced (XBP1us, 164 pb) or spliced (XBP1s, 138 bp) mRNA for X-box binding protein 1 (XBP1) and 28S rRNA (housekeeper) (representative of eight experiments) for cells incubated without (Control) or with tunicamycin as in A. The graph shows XBP1 mRNA/28S rRNA ratio densitometries normalized to 1 in cells from PGMN in the absence of tunicamycin. C. Western blot (representative of eight experiments) for total c-Jun N-terminal kinase 1 (Total JNK1), JNK1 phosphorylated at threonine^{183} and tyrosine^{185} (P~Thr^{183}/Tyr^{185}JNK1), and β-actin as in A. The graph shows Total JNK1/β-actin ratio densitometries normalized to 1 in Control in PGMN. *Lower panel*:

P~Thr^{183}/Tyr^{185}JNK1/Total JNK1 ratio densitometries normalized to 1 in Control in PGMN. *P<0.05 versus Control in PGMN, †P<0.05 versus Control and tunicamycin in PGMO, § and ‡ P<0.05 versus tunicamycin in PGMN and PGMO, respectively, ¶P<0.05 versus Control in PGMO. Values are mean ± S.E.M..

Figure 5. Effect of maternal pre-pregnancy obesity on ATF6-associated endoplasmic reticulum stress marker location in HUVECs. Endothelial cells were isolated from umbilical veins where pregnant women were with a normal pre-pregnancy body mass index (PGMN, *n* = 8 different women) or with pre-pregnancy obesity (PGMO, *n* = 8 different women). Cells were exposed (8 h) to culture medium without (Control) or with tunicamycin (5 μmol/L, inducer of endoplasmic reticulum stress), tauroursodeoxycholic acid (TUDCA, 100 μmol/L, reducer of endoplasmic reticulum stress), or both (see Materials and methods). Confocal microscopy immunofluorescence of activating transcription factor 6 (ATF6) (red fluorescence) and nuclei (blue fluorescence, counterstained with DAPI) was assayed. Fifteen confocal images were taken through the Z-axis (each 0.3 μm) from the bottom to the top of the cells (see Materials and methods). A. Pictures represent Z-stacked images (15 images). B. Pictures show the Z-plane for the optical slide number 7, i.e., ~2.1-2.4 μm from cell culture surface. An amplification is shown at the inserts in each picture. Bars are for all corresponding pictures at 60X microscopy magnifications. Negative control for ATF6 (i.e., without antibody against ATF6) and DAPI in cells from PGMN. C. Immunofluorescent signal at the nuclear over the perinuclear region (see Materials and methods). **P*<0.05 versus Control in PGMN, †*P*<0.05 versus Control and tunicamycin in PGMO, § and ‡ *P*<0.05 versus tunicamycin in PGMN and PGMO, respectively. Values are mean ± S.E.M..

Figure 6. The potential involvement of pre-pregnancy maternal obesity-induced endoplasmic reticulum stress in human umbilical vein endothelial cell dysfunction. Pre-pregnancy maternal obesity (PGMO) associates with an increase (⇧) in the expression and activity of markers of endoplasmic reticulum stress in human umbilical vein endothelial cells. Among these markers, activation of the protein kinase RNA-like endoplasmic reticulum kinase (PERK) and its downstream targets the eukaryotic initiation factor 2 (eIF2α), C/EBP homologous protein 10 (CHOP), and tribbles-like protein 3 (TRB3) is seen in cells from PGMO. This maternal condition also increased total protein abundance but not the phosphorylation at serine^{724} of the inositol-requiring enzyme 1α (IRE1α). PGMO associated with higher phosphorylation of c-Jun N-terminal kinase 1 (JNK1), a downstream target of IRE1α. The location of the activating transcription factor 6 (ATF6) was preferentially in a nuclear region in cells from PGMO. The reducer of endoplasmic reticulum stress tauroursodeoxycholic acid blocked PGMO effects in PERK signalling and ATF6 preferential location in the nuclear region. PERK–eIF2α–CHOP–TRB3 signalling decreased (⇩) the activity of endothelial nitric oxide synthase (eNOS) leading to a lower level of NO paralleled by an increase in the L-arginine transport via the human cationic amino acid transporter 1 (hCAT-1) expression and maximal transport capacity for L-arginine in HUVECs from PGMO. The modulation of L-arginine transport and NO synthesis is mediated by still unknown (?) mechanisms. Green arrows refer to activation and large orange arrows represent a biological effect of PERK and IRE1α signalling.

Table 1. Clinical characteristics of pregnant women and the newborns

Variables	PGMN (*n* = 20)	PGMO (*n* = 22)
Maternal variables		
Age (years)	29.3 ± 4.3 (24–37)	30.6 ± 5.7 (21–45)
Height (cm)	161 ± 5 (152–170)	158 ± 5 (148–171)
Weight (kg)		
Pre-pregnancy [a]	56.0 ± 6.5 (45–65)	83.5 ± 16.6 * (70.2–127)
1st trimester	57.1 ± 6.0 (45.5–65.5)	83.3 ± 18.3 * (65–127)
2nd trimester	64.1 ± 3.1 (59.6–70)	87.5 ± 18.6 * (67.5–130)
3rd trimester	66.9 ± 6.4 (51–74)	90.0 ± 18.1 * (70–132)
Delivery	70.6 ± 5.1 (56.8–83)	90.2 ± 14.8 * (72–135)
ΔGWG (kg)		
Total [b]	14.6 ± 3.9 (11.8–18.0)	6.7 ± 4.0 * (5.0–9.0)
Pre-pregnancy to 1st trimester	1.1 ± 1.3 (0.5–2.5)	-0.2 ± 0.5 * (-0.9–1)
1st to 2nd trimester	7.0 ± 1.1 (5.0–8.2)	4.2 ± 1.4 * (1.5–5.0)
2nd to 3rd trimester	2.8 ± 2.6 (2.0–5.0)	2.5 ± 2.7 (1.5–6.0)
3rd trimester to delivery	3.7 ± 2.1 (2.0–6.2)	0.2 ± 2.3 * (0.0–1.5)
*r*GWG (kg/week) [c]		
Pre-pregnancy to 1st trimester	0.09 ± 0.10 (0.04–0.21)	-0.02 ± 0.03 * (-0.08–0.08)
1st to 2nd trimester	0.58 ± 0.08 (0.42–0.68)	0.35 ± 0.10 * (0.10–0.42)
2nd to 3rd trimester	0.23 ± 0.21 (0.17–0.42)	0.21 ± 0.22 (0.13–0.20)
3rd trimester to delivery	0.31 ± 0.18 (0.17–0.52)	0.02 ± 0.20 * (0.05–0.13)
BMI (kg/m^2)		
Pre-pregnancy [d]	22.1 ± 2.1 (18.7–24.4)	32.8 ± 5.1 * (30.0–50.9)
1st trimester	22.5 ± 1.2 (21.1–24.6)	32.1 ± 4.1 * (30.0–52.0)
2nd trimester	24.6 ± 1.6 (22.9–27.9)	32.5 ± 4.1 * (30.1–42.8)
3rd trimester	26.1 ± 2.0 (21.8–28.4)	33.7 ± 3.8 * (31.2–45.4)
Delivery	27.4 ± 1.3 (24.3–28.9)	35.9 ± 5.0 * (32.0–54.1)
ΔBMI (kg/m^2)		
Total [e]	5.3 ± 0.4 (2.0–7.7)	3.1 ± 0.5 * (2.1–7.4)
Pre-pregnancy to 1st trimester	0.4 ± 0.1 (0.1–1.0)	-0.7 ± 0.1* (-1.2–0.5)
1st to 2nd trimester	2.1 ± 0.1 (1.2–3.1)	0.4 ± 0.1 * (0.2–0.8)
2nd to 3rd trimester	1.5 ± 0.1 (0.8–2.9)	1.2 ± 0.1 (0.7–1.8)
3rd trimester to delivery	1.3 ± 0.1 (0.6–2.5)	2.2 ± 0.3 * (1.6–2.9)
Blood pressure at 1st trimester (mmHg)		
Systolic	104 ± 11 (90–122)	111 ± 12 (90–129)
Diastolic	63 ± 10 (50–78)	70 ± 8 (60–80)
Mean	84 ± 10 (70–98)	90 ± 10 (75–105)
Blood pressure at 2nd trimester (mmHg)		
Systolic	102 ± 10 (85–115)	111 ± 8 (100–120)
Diastolic	63 ± 8 (50–70)	66 ± 5 (60–70)
Mean	82 ± 8 (70–90)	88 ± 6 (80–95)
Blood pressure at 3rd trimester (mmHg)		
Systolic	108 ± 11 (90–125)	113 ± 9 (100–120)

Diastolic	70 ± 8 (60–85)	72 ± 7 (60–80)
Mean	89 ± 8 (75–105)	92 ± 7 (80–100)
Basal glycaemia at delivery (mg/dL)	79 ± 4 (73–85)	78 ± 6 (69–94)
OGTT (mg/dL)		
Glycaemia basal	76 ± 5 (68–85)	77 ± 9 (67–95)
Glycaemia 2 h after glucose load	93 ± 19 (56–125)	99 ± 20 (60–135)
Newborn variables		
Sex (female/male)	11/9	10/12
Gestational age (weeks)	39.3 ± 1.1 (37.1–41)	39.3 ± 1.0 (37.7–40.9)
Birth weight (grams)	3263 ± 274 (2810–3750)	3345 ± 304 (2770–3980)
Height (cm)	50.2 ± 1.5 (48–54)	50.1 ± 1.4 (48–53)
Ponderal index (grams/cm^3 x 100)	2.6 ± 0.2 (2.2–3)	2.7 ± 0.3 (2.3–3.1)
Umbilical vein glycaemia (mg/dL)	64.8 ± 1.8 (48.6–73-9)	68.5 ± 1.8 (57.7–77.5)

Pregnant women were with a normal pre-pregnancy with a normal pre-pregnancy body mass index (BMI 18.5–24.9 kg/m^2) (PGMN) or with pre-pregnancy obesity (BMI ≥30 kg/m^2) (PGMO) according to the US Institute of Medicine guidelines (IOM, 2009). [a] Pre-pregnancy weight corresponds to self-reported weight by the pregnant women at their first interview with the medical specialist (i.e., 9–19 weeks of pregnancy) or the annotated weight in clinical charts after routine medical screening (i.e., 2–3 months before pregnancy). Maternal weight was measured at the 1st (0–14 weeks of gestation), 2nd (14–28 weeks of gestation), 3rd (28–40 weeks of gestation) trimesters of pregnancy and at delivery (37.1–41 weeks of gestation). [b] The total change in gestational weight gain (ΔGWG Total) corresponds to the difference between the weight at pre-pregnancy and delivery. [c] Rates of GWG (*r*GWG) corresponds to ΔGWG (kg)/12 (weeks). [d] Pre-pregnancy BMI was calculated using the pre-pregnancy weight. [e] The total change in BMI (ΔBMI Total) corresponds to the difference between the BMI at pre-pregnancy and delivery. Oral glucose tolerance test (OGTT) (75 g glucose) was measured between 24–28 weeks of gestation. Values are mean ± S.D. (range). *P<0.05 versus corresponding values in PGMN.

Table 2. Kinetic parameters for L-arginine transport in HUVECs from PGMN and PGMO pregnancies

	Saturable transport			*Overall transport*	
	V_{max} (pmol/µg protein/ min)	K_m (µmol/L)	V_{max}/K_m (pmol/µg protein/ min/(µmol/L))	K_D (pmol/µg protein/ min/(µmol/L))	v_i (pmol/µg protein/ 0.5 s)
PGMN					
Control	3.86 ± 0.29	195 ± 42	0.0198 ± 0.0029	0.0081 ± 0.0042	0.0069 ± 0.0001
Tunicamycin	9.50 ± 0.30 *	220 ± 45	0.0432 ± 0.0094 *	0.0109 ± 0.0025	0.0150 ± 0.0001*
TUDCA	4.85 ± 0.35	224 ± 35	0.0217 ± 0.0025	0.0099 ± 0.0013	0.0075 ± 0.0002
Tunicamycin + TUDCA	4.06 ± 0.43	152 ± 51	0.0267 ± 0.0058	0.0114 ± 0.0018	0.0088 ± 0.0001
PGMO					
Control	7.26 ± 0.59 *	253 ± 58	0.0287 ± 0.0043 *	0.0021 ± 0.0010 *	0.0099 ± 0.0001 *
Tunicamycin	7.67 ± 0.49 *	193 ± 36	0.0397 ± 0.0049 *	0.0102 ± 0.0031 †	0.0102 ± 0.0002 *
TUDCA	4.71 ± 0.63 †	203 ± 77	0.0023 ± 0.0005 †	0.0084 ± 0.0026 †	0.0070 ± 0.0002 †
Tunicamycin + TUDCA	4.06 ± 0.10 †	271 ± 18	0.0015 ± 0.0001 †	0.0064 ± 0.0005 †	0.0052 ± 0.0002 †

Legend for Table 2 in the next page.

Legend for Table 2

L-Arginine transport was measured in HUVECs from women with a normal pre-pregnancy body mass index (BMI 18.5–24.9 kg/m^2) (PGMN, n = 12 different women) or from women with pre-pregnancy obesity (BMI ≥30 kg/m^2) (PGMO, n = 12 different women). Cells were coincubated (8 h) in the absence (Control) or presence of tunicamycin (5 μmol/L, an inducer of endoplasmic reticulum stress) and/or tauroursodeoxycholic acid (TUDCA, 100 μmol/L, a reducer of endoplasmic reticulum stress) (see Materials and methods). Saturable transport of L-arginine was derived by subtracting the non-saturable, linear component of transport in the range of L-arginine concentrations used in this study from the overall transport (see Materials and methods). Maximal velocity (V_{max}) and apparent Michaelis-Menten constant (K_m) of saturable transport were calculated assuming a single Michaelis-Menten hyperbola. V_{max}/K_m represents maximal L-arginine transport capacity. The linear phase of overall transport of L-arginine (K_D) was obtained from transport data fitted to a Michaelis-Menten equation increased in a linear component. Initial velocity (v_i) was calculated for 0.5 s with 100 μmol/L L-arginine transport. *P<0.05 versus all other corresponding values in *PGMN*. †P<0.05 versus corresponding Control or Tunicamycin values. Values are mean ± S.E.M..

Highlights

- Pre-pregnancy maternal obesity (PGMO) induces ER stress in HUVECs
- PGMO increases PERK and IRE1α activity, and ATF6 nuclear localization in HUVECs
- PERK targets eIF2α, CHOP, and TRB3 are activated/overexpressed in HUVECs from PGMO
- TUDCA blocked the PGMO-lower NO synthesis and higher L-arginine transport in HUVECs
- PGMO-induced ER stress results in foetoplacental endothelial dysfunction at birth

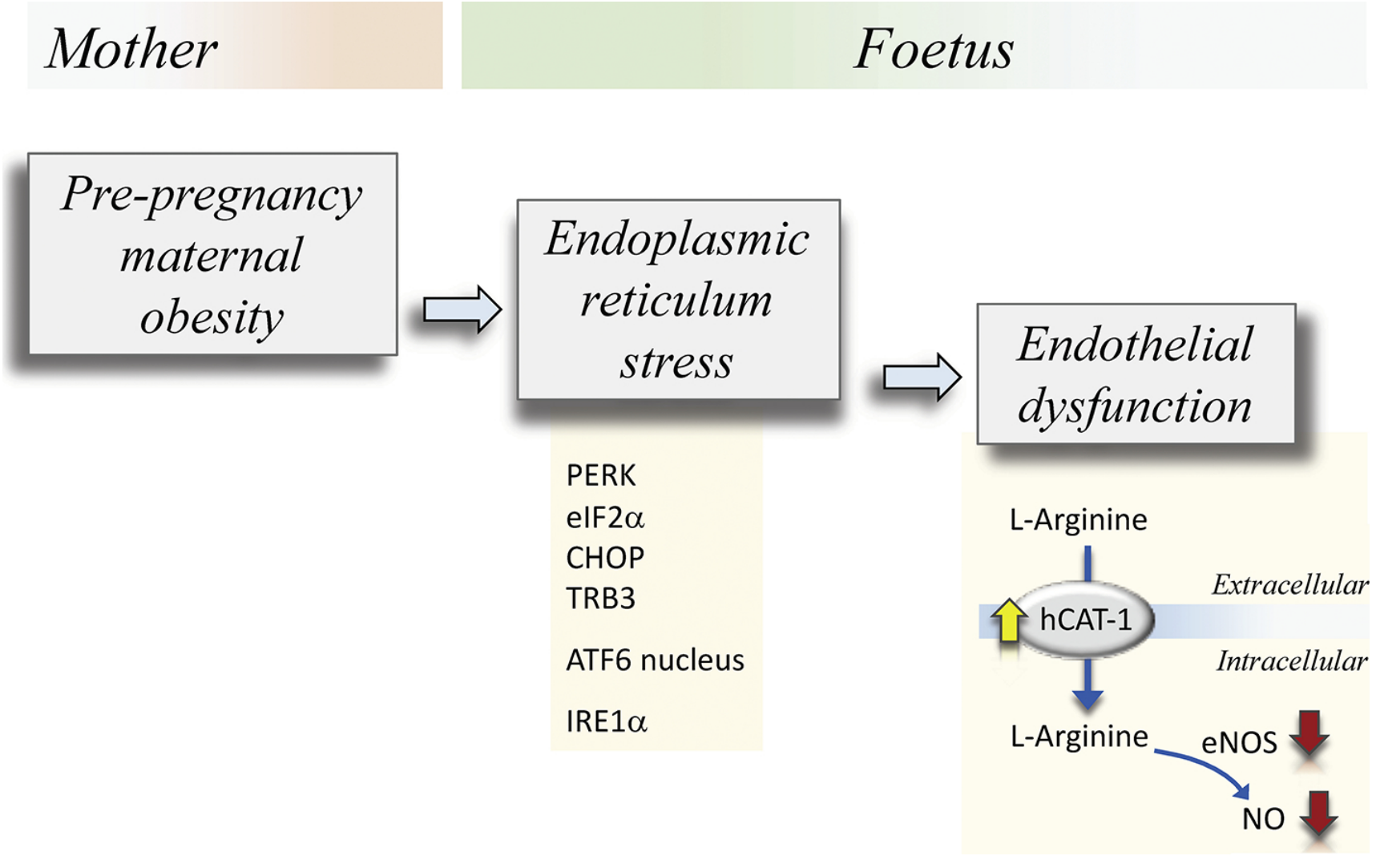

Graphics Abstract

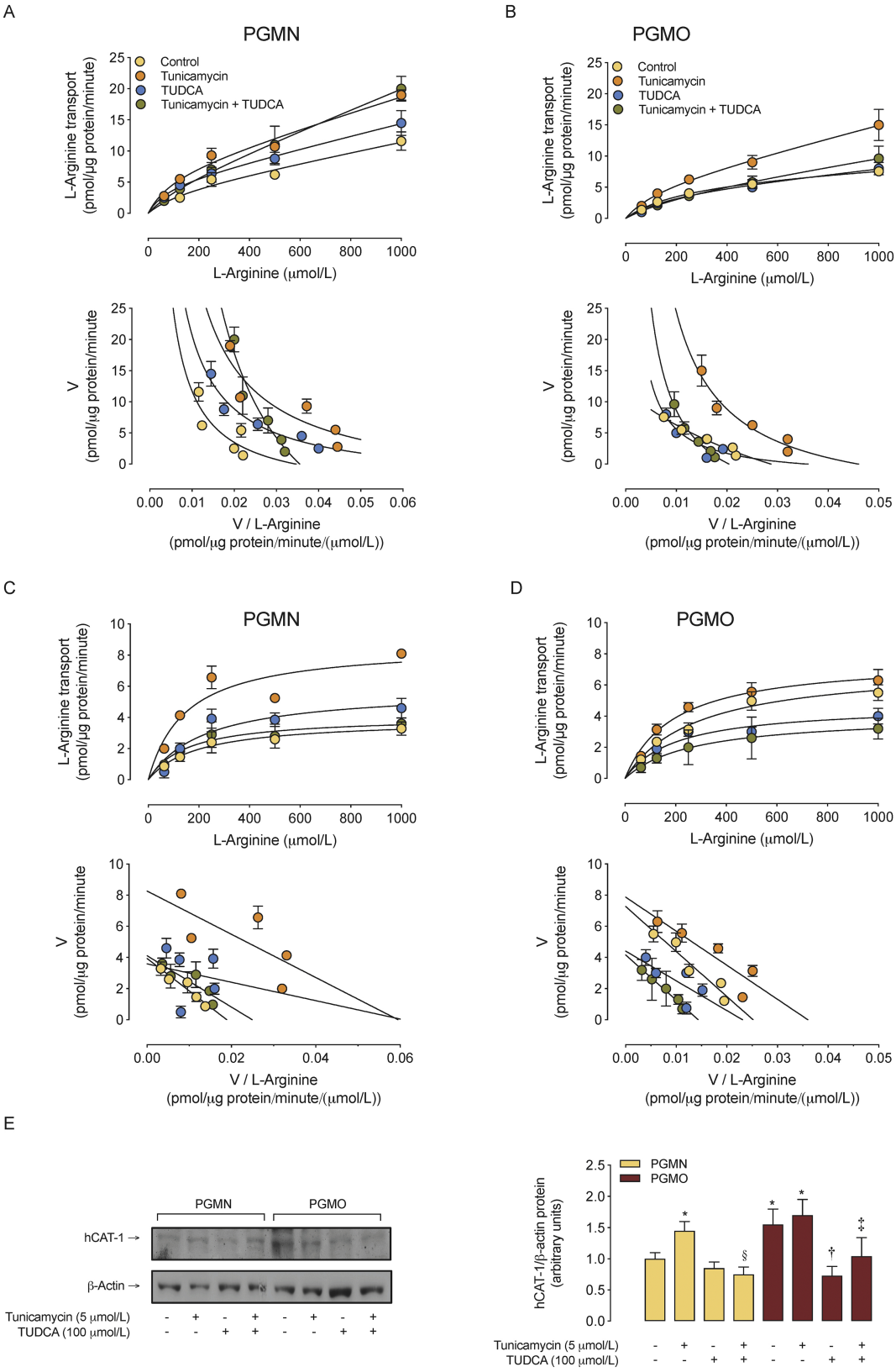
A
PGMN
Control
Tunicamycin
TUDCA
Tunicamycin + TUDCA
L-Arginine transport (pmol/μg protein/minute)
L-Arginine (μmol/L)
V (pmol/μg protein/minute)
V / L-Arginine (pmol/μg protein/minute/(μmol/L))
B
PGMO
C
PGMN
D
PGMO
E
PGMN
PGMO
hCAT-1 →
β-Actin →
Tunicamycin (5 μmol/L)
TUDCA (100 μmol/L)
hCAT-1/β-actin protein (arbitrary units)

Figure 1

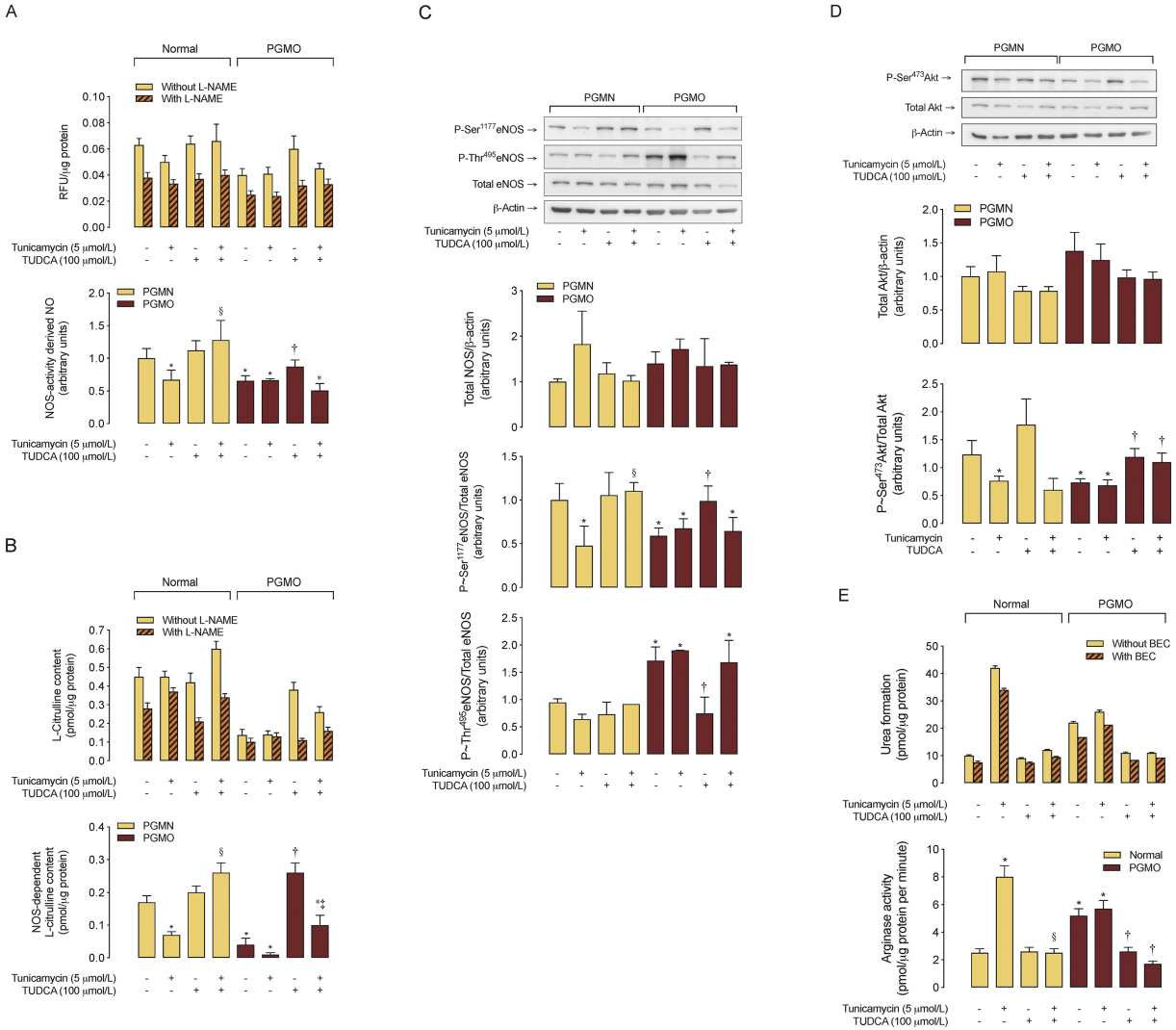
A
Normal
PGMO
Without L-NAME
With L-NAME
RFU/μg protein
Tunicamycin (5 μmol/L)
TUDCA (100 μmol/L)
PGMN
PGMO
NOS-activity derived NO (arbitrary units)
B
L-Citrulline content (pmol/μg protein)
NOS-dependent L-citrulline content (pmol/μg protein)
C
PGMN
PGMO
P-Ser1177eNOS
P-Thr495eNOS
Total eNOS
β-Actin
Total NOS/β-actin (arbitrary units)
P-Ser1177eNOS/Total eNOS (arbitrary units)
P-Thr495eNOS/Total eNOS (arbitrary units)
D
P-Ser473Akt
Total Akt
β-Actin
Total Akt/β-actin (arbitrary units)
P-Ser473Akt/Total Akt (arbitrary units)
Tunicamycin
TUDCA
E
Normal
PGMO
Without BEC
With BEC
Urea formation (pmol/μg protein)
Arginase activity (pmol/μg protein per minute)

Figure 2

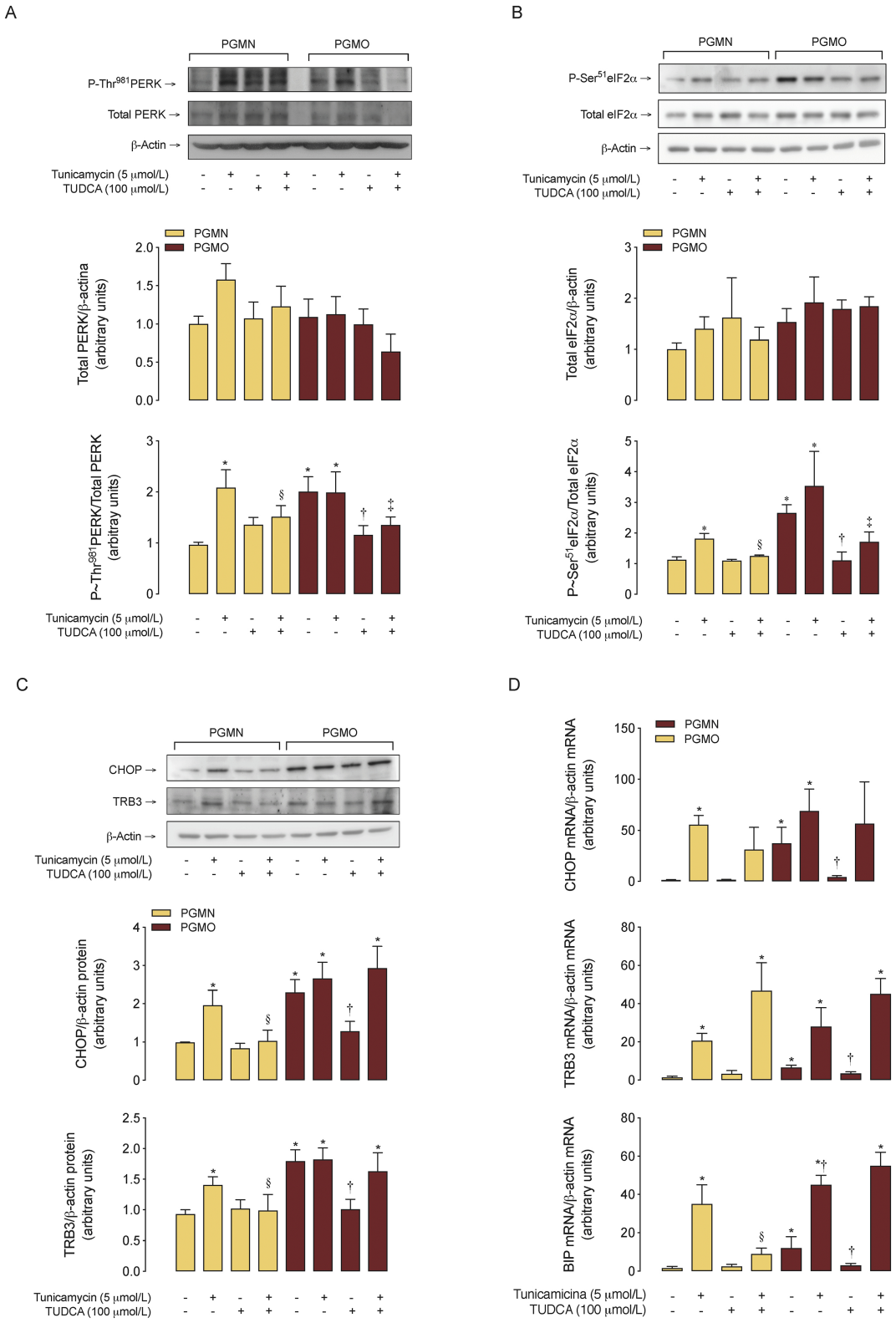
A
PGMN
PGMO
P-Thr981PERK →
Total PERK →
β-Actin →
Tunicamycin (5 μmol/L)
TUDCA (100 μmol/L)
Total PERK/β-actina (arbitrary units)
P~Thr981PERK/Total PERK (arbitray units)
B
P-Ser51eIF2α →
Total eIF2α →
β-Actin →
Total eIF2α/β-actin (arbitrary units)
P~Ser51eIF2α/Total eIF2α (arbitrary units)
C
CHOP →
TRB3 →
β-Actin →
CHOP/β-actin protein (arbitrary units)
TRB3/β-actin protein (arbitrary units)
D
CHOP mRNA/β-actin mRNA (arbitrary units)
TRB3 mRNA/β-actin mRNA (arbitrary units)
BIP mRNA/β-actin mRNA (arbitrary units)
Tunicamicina (5 μmol/L)

Figure 3

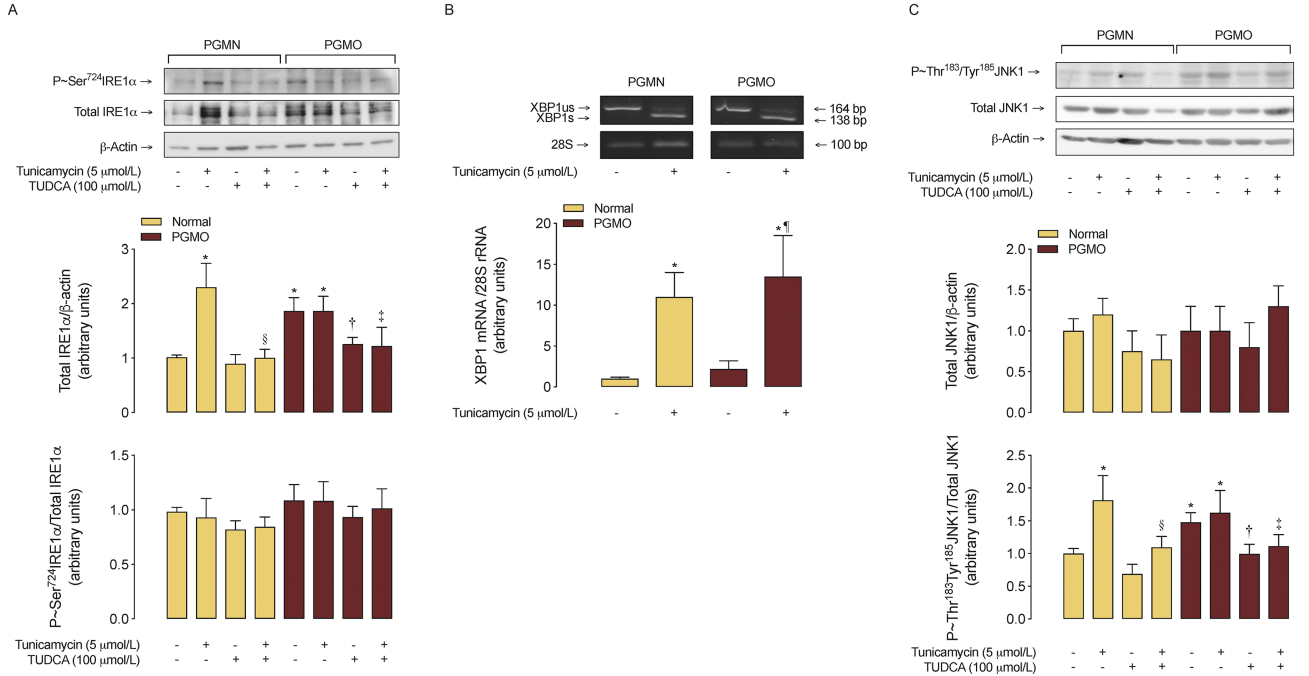
A
PGMN
PGMO
P~Ser724IRE1α →
Total IRE1α →
β-Actin →
Tunicamycin (5 μmol/L)
TUDCA (100 μmol/L)
Normal
PGMO
Total IRE1α/β-actin (arbitrary units)
P~Ser724IRE1α/Total IRE1α (arbitrary units)
B
XBP1us →
XBP1s →
28S →
← 164 bp
← 138 bp
← 100 bp
XBP1 mRNA /28S rRNA (arbitrary units)
C
P~Thr183/Tyr185JNK1 →
Total JNK1 →
Total JNK1/β-actin (arbitrary units)
P~Thr183Tyr185JNK1/Total JNK1 (arbitrary units)

Figure 4

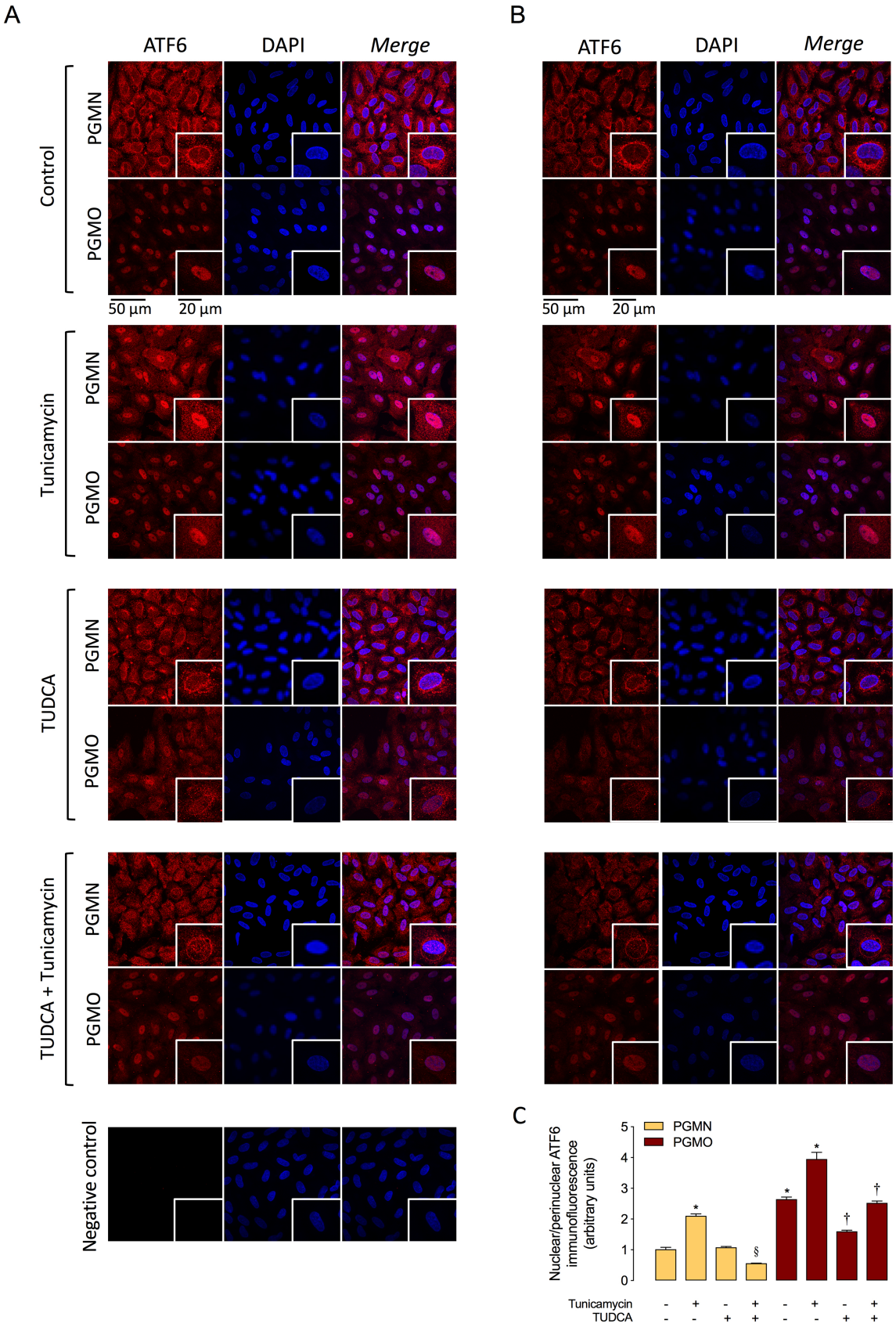
A
B
ATF6
DAPI
Merge
Control
Tunicamycin
TUDCA
TUDCA + Tunicamycin
PGMN
PGMO
50 µm
20 µm
Negative control
C
Nuclear/perinuclear ATF6 immunofluorescence (arbitrary units)
PGMN
PGMO
Tunicamycin
TUDCA

Figure 5

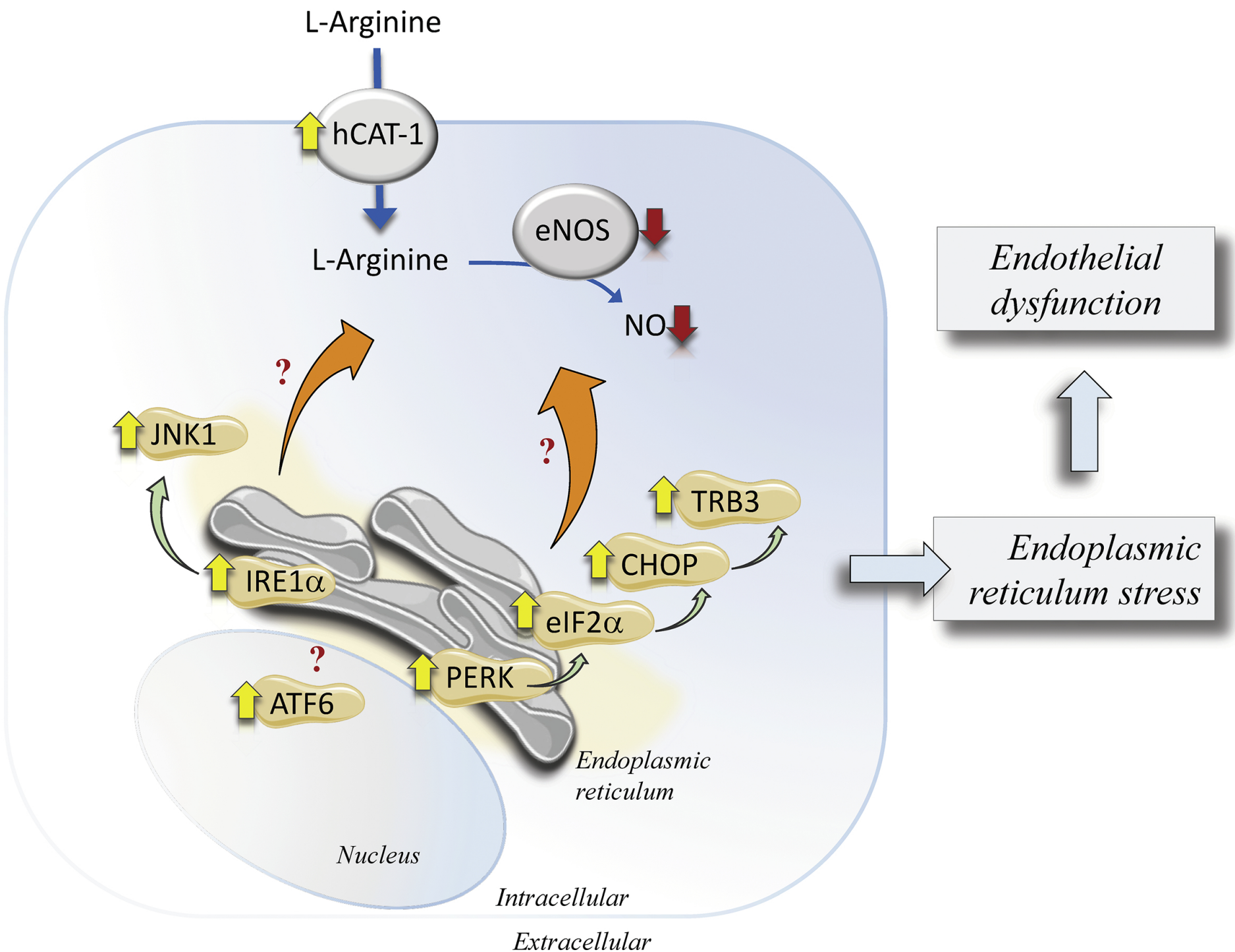
L-Arginine
hCAT-1
L-Arginine
eNOS
NO
?
?
JNK1
TRB3
CHOP
IRE1α
eIF2α
?
PERK
ATF6
Endoplasmic reticulum
Nucleus
Intracellular
Extracellular
Endothelial dysfunction
Endoplasmic reticulum stress

Figure 6